Article type: Review Article

Out of the blue: Semiconductor laser pumped visible rare-earth doped lasers

Christian Kränkel[1,2,], Daniel-Timo Marzahl[1], Francesca Moglia[3], Günter Huber[1,2], and Philip Werner Metz[1]*

*Corresponding author: E-mail: *kraenkel@physnet.uni-hamburg.de*

[1]Institut für Laser-Physik, Universität Hamburg, Luruper Chaussee 149, 22761 Hamburg, Germany
[2]The Hamburg Centre for Ultrafast Imaging, Universität Hamburg, Luruper Chaussee 149, 22761 Hamburg, Germany
[3]Deutsches Elektronen-Synchrotron, Notkestraße 85, 22607 Hamburg, Germany

The rise of semiconductor-based pump sources such as $In_xGa_{1-x}N$-laser diodes or frequency-doubled optically pumped semiconductor lasers with emission wavelengths in the blue encourages a revisitation of the rare-earth ions Pr^{3+}, Sm^{3+}, Tb^{3+}, Dy^{3+}, Ho^{3+} and Er^{3+} with respect to their properties as active ions in crystalline solid-state laser materials with direct emission in the visible spectral range. Nowadays, some of these blue-pumped visible lasers compete with Nd^{3+}-lasers in terms of efficiency and direct lasing at various colors from the cyan-blue to the deep red can be addressed in very simple and compact laser setups. This paper highlights the spectroscopic properties of suitable rare-earth ions for visible lasing and reviews the latest progress in the field of blue-pumped visible rare-earth doped solid-state lasers.

1. Introduction

Visible lasers are fascinating. This does not only hold for their applications in everyday life, where nowadays upcoming applications such as laser headlights and projectors inherit established gadgets like laser pointers or well-known optical data storage devices. It also holds for various other applications in a wide range of topical areas such as display technology,

medicine, material processing, microscopy and scientific research. In fact, the 2014 Nobel prizes in physics and chemistry were awarded "for the invention of efficient blue light-emitting diodes" [1] and "for the development of super-resolved fluorescence microscopy",[2] respectively. Both prizes illustrate the importance of visible lasers. While the Nobel prize in chemistry highlights the significance of visible lasers in research and imaging applications, the research awarded with the Nobel prize in physics directly culminated in blue-emitting GaN and $In_xGa_{1-x}N$- (InGaN-) based laser diodes [3] which enabled many of the results reviewed here. Last not least, solid state lasers in the visible are simple in alignment, allow for fascinating direct insights into optical phenomena (see **Figure 1**) and are as such ideally suited for teaching and outreach activities.[4]

Despite this obvious need for lasers with emission wavelengths in the visible spectral range, until a few years ago there were not many reports on efficient continuous wave rare-earth doped crystalline lasers with direct emission in the visible.

Interestingly, most rare-earth ions exhibit absorption lines in the blue (see **Figure 2**) and corresponding fluorescence in the visible spectral range. Despite this fact the most famous visible solid-state lasers are frequency-doubled Nd^{3+}-lasers with emission wavelengths around 532 nm in the green. They are widespread in green laser pointers, but in particular the application as pump source for the versatile Ti^{3+}:sapphire laser drove the development of 100 W-class continuous-wave output powers [5, 6] and even higher average powers in pulsed operation mode at 532 nm. [7] Nevertheless, the necessary frequency conversion step from the near-infrared to the green spectral range imposes strong requirements on the stability of the fundamental wavelength laser. This reduces the efficiency and contributes to a certain complexity of these systems, which is reflected in the sensitivity towards misalignment and finally the price of commercial high power systems.

The issues connected to frequency-doubled lasers could be circumvented by solid-state lasers with direct emission in the visible, while maintaining the potential for scaling of the output power to comparable levels. In the past, the main obstacle for efficient lasers in the visible was the lack of suitable pump sources with even shorter wavelengths. Initially, inefficient flash-lamps, complex and expensive Ar^+-lasers or toxic dye lasers served as pump sources for visible lasers. This allowed for the realization of visible laser operation, but often these lasers were pulsed and operated at very low efficiency and (average) output power.

The rise of novel pump sources based on semiconductor gain materials such as the InGaN-laser diodes (InGaN) mentioned above [3] and frequency-doubled optically pumped semiconductor lasers (2ω-OPSL) utilizing InGaAs as the semiconductor gain material [10-12] motivated a revisitation of rare-earth doped crystalline solid state laser materials with respect to their suitability for lasers in the visible spectral range.

Nowadays, GaN diodes provide watt-level output powers with reasonable beam quality in the wavelength range around 390 nm. By the admixture of In, InGaN-semiconductors can cover the wavelength range between 390 nm and 460 nm.[3] Even longer wavelengths are possible to be reached, but progress here is hampered by the low miscibility of InN and GaN.[13] In particular in the Blu-ray wavelength range around 405 nm and at wavelengths around 450 nm (see **Figure 3**) used for display applications, such laser diodes with up to 1.5 W of output power are commercially available at very low prices and output power levels of up to 3.5 W are possible [14]. A further scaling of the output power is complicated by difficulties in the growth of large InGaN films of high quality due to the lack of suitable substrate materials and the resulting need for buffer layers.[15] Even at the available maximum output powers the beam quality is reduced significantly. Nevertheless, due to the polarized nature of the output of these diodes, the total

pump power can be increased to more than 10 W by polarization coupling.[14, 16] A further scaling is possible by implementing single diodes into fiber coupled diode laser modules.

2ω-OPSLs, also known as frequency-doubled VECSELs [10], are based on semiconductor gain materials with emission wavelengths around 1 µm. Instead of the common electric pumping of semiconductor lasers, these lasers rely on few µm thick disks, which are optically pumped by laser diodes. Lasing is obtained perpendicular to the surface of the disks in an external cavity, in which a non-linear medium is placed for efficient intracavity frequency doubling into the visible spectral range.[17] In this way, more than 10 W of output power in the green and more than 5 W of output power at wavelengths between 470 nm and 490 nm in the blue can be obtained with excellent beam quality and narrow emission bandwidth (see Figure 3).[12] Obviously, 2ω-OPSLs still rely on a frequency conversion step, but due to their good beam quality they are ideally suited to investigate the laser properties of materials with sufficient absorption in the respective wavelength range. However, the current developments in the field of AlInGaN and In-rich InGaN-based laser diodes extended the emission wavelengths of laser diodes into the green spectral range. This gives rise to the hope that soon also the wavelength range between 470 nm and 490 nm or even beyond can be covered with reliable and affordable pump laser diodes with sufficient output power levels.[13, 18]

In this review, we summarize the latest progress in rare-earth doped lasers in the visible spectral range pumped by semiconductor-based pump sources in the blue. We highlight the advantages and issues imposed by the different rare-earth ions and discuss the requirements on suitable host materials.

2. Spectroscopic properties of rare-earth ions

As mentioned previously, most rare earth ions provide absorption and emission lines in the visible spectral range. In fact, among the 13 optically active rare earth ions, only Ce^{3+}, Gd^{3+}, and Yb^{3+} do not possess any 4f-energy levels allowing for transitions at visible wavelengths.[8] The energy level scheme of Pm^{3+} allows for visible fluorescence, but due to the lack of stable promethium isotopes it is of low practical use for laser applications. Furthermore, Nd^{3+}, Eu^{3+} and Tm^{3+} do exhibit a variety of transitions in the visible and even allowed for visible laser operation. [19-21] However, for Nd^{3+} and Tm^{3+} up to now no reports on direct excitation with blue-emitting semiconductor-based pump sources can be found, while the output power is limited to 2 µW for GaN-pumped Eu:YAG.[21] Therefore, this review focuses on the active rare-earth ions Pr^{3+}, Sm^{3+}, Tb^{3+}, Dy^{3+}, Ho^{3+} and Er^{3+} with their energy level schemes shown in **Figure 4** and **5**. The absorption wavelengths and absorption cross sections of these ions in the blue spectral range are listed in Table 1. Table 2 summarizes their stimulated emission cross sections at the laser transitions and the radiative excited state lifetimes.

2.1. Trivalent praseodymium Pr^{3+}

Trivalent praseodymium is the most established rare-earth ion for the direct generation of visible laser light. It possesses high absorption cross sections exceeding 10^{-19} cm^2 at wavelengths around 445 nm, 470 nm, and 485 nm in typical laser host materials (see **Figure 6**) and an upper state lifetime of several ten microseconds. One of the peak absorption wavelengths matches the emission wavelength of typical InGaN-laser diodes, while a second peak is ideally suited for pumping with 2ω-OPSLs. Compared to other rare-earth ions, the 4f-energy level scheme of Pr^{3+}-ions is not particularly complex (see Figure 4, left). It exhibits various emission lines throughout

the visible spectral range (see **Figure 7**). In the blue, a strong zero-phonon-line emission into the ground state multiplet $^3H_4$ can be found, which can hardly be utilized for efficient laser operation due to the strong reabsorption and the comparably short fluorescence lifetime. However, if the Stark splitting is strong enough, further peaks with cross sections in the order of 10^{-21} cm^2 to 10^{-20} cm^2 may enable quasi-three-level lasing schemes in the blue.[23] The shortest wavelength four-level lasing scheme allows for green laser operation at several weak emission peaks in the wavelength range between 520 nm and 550 nm with cross sections of a few 10^{-20} cm^2. The emission spectrum also exhibits strong peaks in the orange, which, however, suffer from $^3H_4 \rightarrow {}^1D_2$ reabsorption. Despite the spin-forbidden character of this absorption, it features absorption cross sections as high as 3×10^{-20} cm^2 in Pr^{3+}:$LiYF_4$. Fortunately, its peak wavelength at ~595 nm does not overlap with the orange emission lines, thus efficient lasing in the orange is possible. Nevertheless, even the low reabsorption in the order of 10^{-21} cm^2 at wavelengths >600 nm strongly influences the laser properties of orange Pr^{3+}-lasers in particular at low output coupler transmissions, where low absorption losses may become significant during several tens to hundreds of resonator roundtrips for each photon. Moreover, unlike the reabsorption in ground state lasers, this absorption is not bleached at the threshold. The dominant emission in Pr^{3+} is often found in the red around 640 nm, where emission cross sections exceeding 10^{-19} cm^2 can be observed. Further peaks with somewhat lower cross sections are present around 700 nm and 720 nm. Both feature broad phononic sidebands with about one order of magnitude lower cross sections, which is still sufficient to allow for a broad spectral tuning in this wavelength range.

The main issue of Pr^{3+}-doped materials is their sensitivity towards cross relaxation processes with increasing doping concentrations, which depopulates the upper laser level and reduces the effective lifetime of the emitting thermally coupled $^3P_J/^1I_6$-levels. For this reason, the doping

concentration should not exceed ~1.5×10^{20} cm^{-3}, which corresponds to about 1 at.% doping concentration, e.g., in $LiLuF_4$.

Regarding the choice of suitable host materials, two main aspects have to be considered. First, the $^3P_J/^1I_6$-levels of Pr^{3+} are prone to non-radiative phononic decay into the $^1D_2$-multiplet, if the phonon energies of the host lattice are too high. As a rule of thumb the probability for non-radiative multi-phonon decay is uncritical if the energy gap is more than 4 times larger than the maximum phonon energy.[24] Second, the energetic position of the energy levels of the $4f^15d^1$-configuration with respect to the $4f^2$-states is in general low in Pr^{3+}, if compared to other rare-earth ions.[25] This gives rise to excited state absorption (ESA) at the pump and/or the laser wavelength, if the crystal field strength of the host lattice is too high. In this case, the enhanced Stark splitting further decreases the energetic position of the $4f^15d^1$-levels.[26] For this reason, in the past mainly fluoride host materials, which are known for their low phonon energies and a comparably low crystal field strength, served as host materials for visible lasers based on Pr^{3+}. For example Laroche et al. identified the energetic position of the lowest $4f^15d^1$-levels to be beyond 46.000 cm^{-1}, i.e. at wavelengths below 220 nm in several fluoride hosts, thus no ESA should occur at wavelengths >440 nm.[27,28] Nevertheless, there are also reports on efficient laser operation of Pr^{3+} in oxide host materials.[16, 29]

2.2. Trivalent samarium Sm^{3+}

Trivalent samarium offers various absorption peaks in the blue spectral range. The strongest absorption with cross sections in the order of a few 10^{-20} cm^2 can be observed in the wavelength range around 400 nm (see Figure 6). This wavelength range can be conveniently covered by GaN-based laser diodes, which are commercially available for affordable prices due to their wide-spread use in Blu-ray drives. The absorption peaks at longer wavelengths are all spin-

forbidden and thus exhibit roughly one order of magnitude lower cross-sections. As an example, the absorption around 480 nm, which can be addressed by 2ω-OPSLs, shows absorption cross sections of a few 10^{-21} cm^2, e.g., in $LiLuF_4$ [30] or $LiYF_4$ [31] but also in oxide materials.[32]

Unfortunately, the complex energy level scheme of the $4f^5$-configuration of Sm^{3+} (see Figure 4, middle) is prone to cross-relaxation processes which quench the lifetime [33] at doping concentrations exceeding ~4×10^{20} cm^{-3} (i.e. ~3 at.% in $LiLuF_4$). Therefore, pumping at the higher peak absorption around 400 nm is desirable to achieve efficient pump light absorption in the laser crystal.

The fluorescence spectrum of Sm^{3+} (see Figure 7) exhibits several peaks in the visible, which arise from transitions from the $^4G_{5/2}$ into the ^6H_J-levels and are also spin-forbidden. The main emission bands in the visible, noted in decreasing order of intensity, can be found in the orange around 600 nm, in the red around 650 nm, in the deep-red around 700 nm, and in the green around 560 nm. The peak emission cross sections in the orange approach 10^{-21} cm^2, while only a few 10^{-22} cm^2 are observed in the green. A further consequence of the spin-flip in all fluorescence transitions from the $^4G_{5/2}$-multiplet is a very long upper state radiative lifetime in the order of a few milliseconds.[30, 32]

As the energetic position of the 5d-levels is in general higher in Sm^{3+} compared to Pr^{3+},[25] ESA into these levels should not impose a problem here, even in host materials with a stronger crystal field. Also with respect to the phonon energies the selection of the host material is rather uncritical, as the energetic gap below the emitting level $^4G_{5/2}$ is larger than 6000 cm^{-1}. Therefore, Sm^{3+} should be less sensitive towards the host material and oxide crystals can be considered. However, the complex energy level scheme may strongly support ESA, energy upconversion and cross relaxations [33] in unsuitable host crystals.[34]

2.3. Trivalent terbium Tb^{3+}

In the energy level scheme of Tb^{3+}, the $^5D_4$- as well as the $^5D_3$-multiplet can be considered as an upper laser level (see Figure 4, right). The energy gap of ~5500 cm^{-1} between the two would require quite high phonon energies to allow for non-radiative multi-phonon relaxation with an order below 4.[24] Unfortunately, this energy gap features efficient cross relaxation from the ground state $^7F_6$ into one of the higher lying ^7F_J-multiplets. The cross relaxation efficiently depopulates the $^5D_3$-multiplet at the required high Tb^{3+}-doping concentrations (see below) and hinders effective energy storage in this multiplet.

In contrast, the $^5D_4$-multiplet does not suffer cross relaxation and exhibits a very long upper state lifetime in the order of 5 ms in typical fluoride host materials even at high doping concentrations. The $^5D_4$-multiplet is accessible via direct in-band pumping at wavelengths around 485 nm [35] (see Figure 6) available from 2ω-OPSLs, but the spin-forbidden $^7F_6 \rightarrow {}^5D_4$-absorption features extremely low cross sections in the order of a few 10^{-22} cm^2.

However, the low absorption cross sections can be partially compensated by high doping concentrations without the risk of concentration quenching of the $^5D_4$-multiplet lifetime. Doping concentrations of a few 10^{21} cm^{-3}, corresponding to several 10 at.% of doping concentration or even stoichiometric full doping at low site densities seem feasible. In this way, absorption coefficients in the order of 1 cm^{-1} can be achieved despite the low absorption cross sections. These high doping concentrations in combination with the long upper state lifetimes and the low cross sections allow for very high stored energy per volume, making this ion also potentially attractive for q-switched operation with high pulse energies.

The efficient de-excitation of the upper multiplet $^5D_3$ by cross relaxation also enables a four-level pumping scheme. In this case, pump sources around 380 nm would be required. This approach

benefits from roughly a factor of 10 higher ground state absorption cross sections at the respective wavelength. As a drawback, such short pump wavelengths would compromise the Stokes efficiency between the pump and the visible laser photons and limit the achievable laser efficiency. Furthermore, pump-ESA into even higher 5d-levels cannot be excluded in this pumping scheme.

The electron configuration of Tb^{3+} corresponds to the highly bound half-filled 4f-shell of Gd^{3+} plus one electron, which can be easily excited into the 5d-shell. Therefore, besides Ce^{3+} with only one 4f-electron, the Tb^{3+}-ion is known to typically exhibit the energetically lowest $4f^{n-1}5d^{1}$-levels,[26, 36] which has been shown to be valid also in $LiYF_4$.[37] Similar to Pr^{3+} and also Ce^{3+}, this should enable ESA into 5d-levels. In fact, these 5d-levels occur as a strong ground state absorption peak around 250 nm in many fluoride host materials. However, the transition from the excited $^5D_4$-multiplet into the lowest ^9D-levels of the $4f^75d^1$-configuration is even doubly spin-forbidden and thus the corresponding ESA is suppressed very strongly despite the parity allowed nature of interconfigurational 4f → 5d transitions.[38, 39]

In fluorescence, Tb^{3+} exhibits mainly three emission peaks around 540 nm, 585 nm, and 620 nm in the green, yellow-orange and red, respectively (see Figure 7). The emission cross sections are in the order of 10^{-21} cm^2 and thus comparable to those in Sm^{3+}-doped materials and surprisingly about one order of magnitude higher than the absorption cross sections at 485 nm.[40]

Despite the low energetic position of their 5d-bands, also oxides can be considered as host materials for Tb^{3+}. Firstly, the energetic position of the lowest singly spin-forbidden 5d-bands is even higher than in Pr^{3+}, which has been shown to be suitable for laser operation in oxides,[16] second, the $^5D_4$-multiplet of Tb^{3+} is not sensitive towards non-radiative transitions enabled by the typically higher phonon energies of oxides.

2.4. Trivalent dysprosium Dy^{3+}

Also in Dy^{3+} all transitions in the visible require a spin flip (see Figure 5, left). Thus, the ground state absorption cross sections from the $^6H_{15/2}$ ground state into the $^4F_{9/2}$, $^4I_{15/2}$, and $^4G_{11/2}$ states at wavelengths around 425 nm, 450 nm and 475 nm are as low as 10^{-21} cm^2 (see Figure 6). The highest peak around 450 nm is suitable for pumping with InGaN-laser diodes, whereas the even lower absorption around 475 nm can be addressed by 2ω-OPSL pump sources. The 4f-shell of Dy^{3+} possesses 5 holes and thus the same number of energy levels as Sm^{3+} with the 4f-shell filled with 5 electrons. Therefore, it is not surprising that Dy^{3+} is also prone to cross-relaxation processes, which limit the maximum doping concentration to ~10^{21} cm^{-3}, corresponding to below 10 at.% in many host materials. Due to the low absorption cross sections, this requires crystal lengths in the order of centimeters to achieve efficient absorption.

The spin forbidden emission cross sections of Dy^{3+} are comparable to those in absorption. Interestingly, the highest emission cross sections of up to 1.5×10^{-21} cm^2 in Dy^{3+}:$LiLuF_4$ are centered around 580 nm in the yellow part of the visible spectrum, where most other ions, except Tb^{3+}, do not exhibit fluorescence suitable for laser operation (see Figure 7). Further emission bands can be found around 660 nm and 750 nm. Here the cross sections are about three to four times lower. The lifetime of the possible upper laser level $^4F_{9/2}$ is in the order of one millisecond in fluoride host materials.[41, 42]

For all non-ground-state transitions the depopulation of the terminal level occurs via the $^6H_{13/2}$-multiplett (see Fig. 5, left), which possesses a significantly long lifetime. Therefore, host materials with high phonon energies may even be beneficial to quench the lifetime of the lower laser levels $^6H_{9/2}$, $^6H_{11/2}$, and $^6H_{13/2}$. Another approach is co-doping with other optically active ions. Energy transfer to short-living energy levels of the co-dopant may support a fast

depopulation of the respective terminal level. When following this approach, co-dopants with resonant cross-relaxation channels for the upper laser level $^4F_{9/2}$ should be avoided, as this may detrimentally quench the upper state lifetime. The energetic position of the lowest energy levels of the $4f^8 5d^1$-configuration of Dy^{3+} is higher than, e.g., in the case of Pr^{3+} and these transitions are doubly spin-forbidden such as in the case of Tb^{3+}.[26] Therefore, oxides can be suitable host materials also for Dy^{3+} [43] and the risk of 5d-ESA is very low. However, as in the case of Sm^{3+}, the variety of 4f-energy levels makes this laser ion prone to ESA or upconversion processes in unsuitable crystal fields.

2.5. Trivalent holmium Ho^{3+}

Ho^{3+} is mainly known for lasers in the 2 µm wavelength range.[44] But it also provides laser transitions in the visible. In fact, its absorption spectrum features cross sections in the order of a few 10^{-20} cm^2 in the wavelength range around 450 nm accessible for blue InGaN-laser diodes (see Figure 6). Even larger absorption cross sections can be found in the green, where frequency-doubled Nd^{3+}-lasers could serve as pump sources for in-band pumping. The absorption cross sections in the emission wavelength range of 2ω-OPSL-pump sources around 480 nm are lower and hardly reach 10^{-20} cm^2. In both cases, the energetic distance to the $^5F_3$-multiplet is low enough to allow for a fast non-radiative decay into the thermally coupled $^5S_2$- and $^5F_4$- multiplets (see Figure 5, middle).[45]

At the first sight, these multiplets may serve as upper laser levels for several four-level schemes, but the de-excitation of all prospective laser terminal-levels happens via the $^5I_7$-multiplet. This multiplet serves as the upper laser level for 2 µm-laser transitions and its lifetime amounts easily up to 10 ms.[44] Thus, population may be trapped in this state, severely increasing the required inversion, e.g., for lasing in the deep-red at 750 nm. Consequently, the only remaining candidate

is the green ground state transition $^5S_2$,$^5F_4$ → $^5I_8$. In Ho^{3+}:$LiLuF_4$, this transition exhibits peak cross sections of up to 2×10^{-20} cm^2 at 535 nm. However, very high inversion is required to reach the laser threshold at this wavelength corresponding to the zero-phonon-line transition. The transitions into the higher Stark levels of this multiplet at wavelengths between 540 nm and 550 nm provide lower cross sections of 0.5×10^{-20} cm^2 (see Figure 7).

Despite these comparably low cross sections, the fluorescence lifetime of the upper laser level is significantly shorter than 1 ms and amounts to only about 100 µs, e.g., for Ho^{3+}:$LiLuF_4$. Detailed investigations revealed, that already at room temperature and in case of the low-phonon-energy host $LiLuF_4$, this lifetime is strongly quenched by non-radiative phonon-assisted transitions via the $^5F_5$-multiplet and further multiplets back into the ground state.[46] Therefore, only very low phonon energy host materials such as heavier halides [47, 48] are regarded to be suitable host materials for visible cw lasers based on Ho^{3+}.

Due to the high energetic position of the lowest $4f^95d^1$ levels ESA is not considered to be a problem in Ho^{3+}-doped materials. However, several intraconfigurational cross-relaxation processes are possible and prevent the use of doping concentrations exceeding a few 10^{19} cm^{-3}, i.e. about 1 at.% in most host materials.

2.6. Trivalent erbium Er^{3+}

Besides the well-known laser transitions in the 1.5 µm [49] and 3 µm range [50, 51] also visible laser transitions can be addressed in Er^{3+}. Typically, these green emitting lasers are pumped via an upconversion pumping scheme,[52, 53] but the absorption spectrum also allows for pumping with blue-emitting semiconductor-based pump sources at wavelengths around 405 nm, 450 nm or 485 nm (see Figure 6). The absorption cross sections for the first two wavelengths are typically in the order of a few 10^{-21} cm^2, but they exceed 1.5×10^{-20} cm^2 in Er:$LiLuF_4$ at 485 nm, where 2ω-

OPSL-pump sources are available. This value is 50 % higher than the absorption at the typical upconversion pump wavelengths around 970 nm. The possibility of detrimental ESA processes at the blue pump wavelengths due to the complicated energy level scheme of Er^{3+} (see Figure 5, right) is present, but not well investigated, yet. In all these pumping schemes, the upper laser level is the $^4S_{3/2}$ level with a radiative upper state lifetime in the order of a few 100 µs in typical host materials.[52]

In emission, Er^{3+} provides cross sections in the order of 10^{-20} cm^2, higher than any other ion presented in this work except Pr^{3+}, at wavelengths around 550 nm in the green spectral range (see Figure 7).[54] Also in Er^{3+} the energetic position of the lowest $4f^{10}5d^1$-energy levels is high enough to suppress 5d-ESA.[25]

Due to lifetime quenching at doping concentrations exceeding ~2×10^{20} cm^{-3}, the doping concentration is limited to about 1.5 at.%, e.g., in $LiYF_4$.[52] The energy gap from the upper laser level $^4S_{3/2}$ to the next lower level $^4F_{9/2}$ is in the order of 3000 cm^{-3}, comparable to the situation in Pr^{3+}. Thus, Er^{3+} is not expected to exhibit non-radiative decay in fluoride host materials. Nevertheless, one order of magnitude shorter $^4S_{3/2}$-lifetimes are observed in oxide host materials compared to fluoride hosts.[55, 56] This may be caused by more resonant cross relaxation processes transferring energy from $^4S_{3/2}$ into the long living $^4I_{13/2}$-multiplet (see Figure 6). Besides quenching the lifetime, the accumulation of energy in this level has destabilizing consequences for the laser process,[57] comparable to the situation in Ho^{3+} described above. Additionally, the stronger crystal field of oxides may decrease the gap between the $^4S_{3/2}$- and the $^4F_{9/2}$-multiplet by a strong Stark splitting, promoting non-radiative decay which also populates the $^4I_{13/2}$-multiplet. Therefore, oxides are not considered to be suitable hosts for Er^{3+}.

3. Laser performance

One of the most common host materials for visible lasers is $LiYF_4$ (YLF). Due to its low phonon energies and low crystal field strengths, this crystal is a suitable host material for most of the laser ions presented in this review. It possesses a tetragonal $I4_1/a$ lattice structure and features reasonable thermo-mechanical properties compared to oxide host materials.[62] However, the growth imposes difficulties. According to some authors, it does not grow from a perfectly stoichiometric melt [63] and it requires even more reducing growth atmospheres, often containing HF,[64] than other fluoride host materials. In contrast, the isostructural $LiLuF_4$ (LLF), featuring very similar spectroscopic and thermo-mechanical properties, can be grown from a stoichiometric melt under less aggressive growth atmospheres.[65] A minor drawback might be the more expensive LuF_3 required as a component for the starting materials and a somewhat lower segregation coefficient for larger rare earth ions such as Pr^{3+}. Our and other research in the past years delivered no evidence that either $LiLuF_4$ or $LiYF_4$ is in general better or worse suited as a host material (see e.g. [66, 67]). In fact, the differences in laser performance of identical material systems from different growth runs would often be larger than the differences between these two host materials. While many researchers depend on the commercially available $LiYF_4$, our results with $LiLuF_4$ as a host material were mainly obtained with crystals grown in our facilities. In the following, we will review the results obtained with rare-earth doped $LiYF_4$ and $LiLuF_4$ crystals, but also highlight outstanding results obtained with other host materials. A summary of the laser parameters obtained with Pr^{3+}, Sm^{3+}, Tb^{3+}, Dy^{3+}, Ho^{3+} and Er^{3+} doped into $LiYF_4$ or $LiLuF_4$ can be found in Table 3.

It should be noted that many outstanding laser results have also been obtained with fiber lasers in particular doped with Pr^{3+} in the past.[68, 69] These lasers benefit from the broad emission

spectra resulting from the disordered glass matrix, which allows for very wide wavelength tuning in the visible, however often at the drawback of very low output power and efficiency.[70] The cw output power of these lasers is limited to less than 1 W up to now,[71] and further scaling seems not to be straightforward due to the weak material properties of the required low-phonon fluoride-fibers. However, glass-fiber hosts will not be part of this review, a good overview on the current state of the art is given e.g. in [71].

3.1. Pr^{3+}-doped lasers

The trivalent praseodymium ion with its bright white fluorescence arising from several emission lines throughout the visible spectral range was among the first ions to be utilized for laser experiments.[78] Nowadays, Pr^{3+}-doped materials represent one of the most efficient approaches to generate visible laser radiation. Though interestingly the first Pr^{3+}-laser emitted at 1047 nm in the infrared,[78] as early as 1963 the first visible laser emitting at 599 nm was demonstrated in Pr^{3+}:LaF_3 under flash-lamp pumping.[79] Up to now Pr^{3+}-doped materials are by far the most examined rare-earth doped crystals for the direct generation of visible laser radiation.

The first results under pumping in the blue were obtained using dye-lasers for pulsed excitation of stoichiometric $PrCl_3$ and $PrBr_3$.[80] This approach even allowed for lasing in the blue at 479 nm in Pr^{3+}:$LiYF_4$.[81] Later, Ar^+-lasers and frequency-doubled Nd^{3+}-ground state lasers served as pump sources for the first blue-pumped continuous wave lasers based on Pr^{3+}-doped $LiYF_3$, KYF_4 and $LiGdF_4$ emitting in the green, orange, red and deep red [82] as well as for the first modelocked Pr^{3+}-lasers.[83, 84] Meanwhile, various other host materials such as the fluorides $LiLuF_4$,[66, 85] KY_3F_{10},[67, 86] BaY_2F_8,[87-89] SrF_2,[90] LaF_3,[91] β-$NaGdF_4$,[92] and β-$Y_{0.5}Gd_{0.5}F_3$ [93] as well as oxides like $YAlO_3$,[94, 95] $LuAlO_4$,[96] $SrAl_{12}O_{19}$,[97, 98] and

$LaMgAl_{11}O_{19}$ [99] are established as host materials for blue-pumped continuous wave visible Pr^{3+}-based lasers. It should be noted, that all the oxides mentioned here provide a 12-fold coordinated lattice site for the Pr^{3+}-ion, which leads to a comparably large distance to the coordinating O^{2-}-ions and results in lower crystal field strengths. The latter prevents a strong decrease of the 5d energy level positions and thus ESA into these levels.[26] In contrast, typical oxide host materials such as garnets [100] or sesquioxides [101] do not provide such highly coordinated sites and are not regarded as suitable host materials for Pr^{3+}.

The rise of InGaN-based laser diodes emitting in the blue [3] enabled the first diode-pumped Pr^{3+}-lasers [86, 95, 102] and even diode-pumped Pr^{3+}-waveguide-lasers in the visible.[103, 104] However, the output power of InGaN-diodes is nowadays limited to about 3.5 W.[14] Fiber coupled diode arrays are available but come at the expense of a significantly reduced beam quality. Moreover, the thermo-mechanical properties of fluorides typically are not suitable for highest pump powers. Accordingly, such fiber-coupled diodes have only been utilized as a pump source for Pr^{3+}:$SrAl_{12}O_{19}$, so far.[105] Very high efficiencies under diode pumping have been obtained under pumping with more than one single emitter from both sides. In this configuration, nearly 1 W of red output at 640 nm could be obtained with only 2 W of incident pump power.[75] Considering the Stokes efficiency of 69 % between the pump photons at 444 nm and the laser wavelength, the slope efficiency of 64 % was close to the maximum possible value. In the same setup, several 100 mW of output power could also been obtained in the green at 523 nm and 546 nm as well as in the orange around 605 nm (See **Figure 8 (left)**), but also the transition at 698 nm is suitable for efficient diode pumped operation (See **Figure 8 (right)**). Recently, using 4 individual laser diodes with an output power of 3.5 W each and combining pumping from both sides with polarization coupling, up to 2.9 W of output power at 640 nm were obtained **(see**

Figure 9).[14] Meanwhile, efficient diode pumped laser operation was also demonstrated in oxide materials such as Pr^{3+}:$YAlO_3$ [29, 95] (See **Figure 10**) and Pr^{3+}:$SrAl_{12}O_{19}$.[16]

Pumping with 2ω-OPSLs emitting around 480 nm allows for even higher efficiencies due to the increased Stokes efficiency. A 2ω-OPSL pumped Pr^{3+}:$LiYF_4$ laser was demonstrated for the first time in 2004.[106] Since then, such pump sources have been utilized in various experiments.[66, 107] Due to the good beam quality of this pump source it is also ideally suited to pump lasers in waveguide geometry. A photography of such a visibly emitting waveguide laser is shown in Figure **9**.[108-110]

Up to now, the best results have been obtained with Pr^{3+}:$LiYF_4$. Slope efficiencies in excess of 70 % at 523 nm and in the red at 640 nm were demonstrated (see **Figure 12a**).[73] The same material enabled more than 4 W of output power at 523 nm in the green under pumping with more than 10 W of blue radiation from two 2ω-OPSLs (see **Figure 13**).[74]

Due to very low laser thresholds in these four level laser schemes, the highest optical-to-optical efficiencies were well above 60 % even with respect to the incident pump power (see **Figure 12b**). In the same experimental setup, efficient lasing with more than 40 % of slope efficiency and more than 1 W of output power could also been obtained at five further wavelengths in the green, orange, red and dark red spectral range (cf. Figure 12).[73]

The potential of Pr^{3+}-doped crystals for cyan-blue emission based on quasi-three-level lasing schemes has been realized early, but due to the higher inversion needed to overcome the lasing threshold compared to a four-level laser scheme, for a long time lasing on the ground state transition was only obtained under pulsed excitation.[23, 81, 111] Very recently, continuous wave lasing in the cyan-blue range was obtained with Pr^{3+}:BaY_2F_8 at 495 nm as well as with Pr^{3+}:$LiYF_4$ at 491 nm and 500 nm (see **Figure 14**). Up to now, the best results were obtained

utilizing Pr^{3+}:BaY_2F_8 under 2ω-OPSL-pumping. In this case, the slope efficiency was 27 % and an output power of 200 mW could be obtained. Successful experiments were also carried out under InGaN-diode pumping.[72, 112]

Lasers with direct emission in the visible spectral range allow for the efficient generation of UV radiation via simple intracavity frequency doubling. Utilizing a 2ω-OPSL as the pump source, up to 1.3 W and 0.36 W of continuous wave output power could be generated at 360 nm [113] and 320 nm, respectively, by frequency doubling of the deep-red and red transitions at 720 nm and 640 nm in Pr^{3+}:$LiYF_4$.[66] In both cases, the optical-to-optical efficiency with respect to the absorbed pump power was significantly higher than 20 %. Even shorter emission wavelengths were demonstrated using two 2ω-OPSLs to pump the green Pr^{3+}:$LiYF_4$ laser at 523 nm. Under pumping with a total of 10 W of pump power, 1 W of continuous laser output at 261 nm was demonstrated.[74] Similar experiments were also conducted under pumping with two InGaN-laser diodes. Using only 2 W of incident pump power, 0.48 W of UV radiation at 261 nm were generated. With respect to the incident pump power, the efficiency was 26 % in these experiments. Considering only the absorbed pump power, the efficiency amounted even to 37 %.[114] Also other wavelengths can be considered for frequency doubling, if particular wavelengths in the UV are required. As an example, initial experiments were performed on intracavity frequency doubling of 546 nm to 273 nm [115] and 698 nm to 349 nm.[116] Besides Pr^{3+}:$LiLuF_4$,[117] frequency doubling of Pr^{3+}-lasers in other host materials such as Pr^{3+}:KY_3F_{10},[118] Pr^{3+}:BaY_2F_8,[87] and Pr^{3+}:$YAlO_3$ [119] did not result in efficient generation of coherent UV radiation, yet. However, this should not be a general issue of these host materials.

Even though the emission spectrum of Pr^{3+} is dominated by several prominent peaks (see Figure 7), a broad phononic background can be found in particular in the red part of the spectrum. The

cross sections in the order of 10^{-21} cm^2 of this background are still larger than the peak cross sections of other ions presented in this review. This also enables continuous tuning of the emission wavelength around these peaks. Initially, this range was restricted to a few nanometers around the peaks,[84, 91, 120] but recently a total tuning range of nearly 100 nm covering wide parts of the red, orange and green region of the visible spectrum was demonstrated in Pr^{3+}:KY_3F_{10} (see **Figure 15 a**).[121] Using a 1.2 W InGaN-laser diode emitting at 445 nm as a pump source, a continuous tuning range of 50 nm between 687 nm and 737 nm could be realized in the dark red. Also in the orange around 615 nm and in the red around 650 nm tuning ranges in the order of 20 nm were obtained. In these experiments, the pump was chopped to avoid thermal depolarization and the q-cw output power was limited to less than 200 mW. However, these initial experiments showed that Pr^{3+}-doped crystals are suitable for broad continuous wave tuning ranges and the possibility to generate laser operation at a large variety of distinguished emission wavelengths. In other host materials with more pronounced emission peaks compared to Pr^{3+}:KY_3F_{10} it is often difficult to obtain wavelength tuning around the largest peaks, e.g., at 640 nm, because emission at the peak wavelength cannot be suppressed sufficiently. If particular wavelengths are required, this problem can easily be solved by special coatings or volume Bragg gratings.[122] Meanwhile, we succeeded in obtaining broad true cw tuning ranges also with Pr^{3+}:BaY_2F_8 (**Figure 15 b and c**), which even allowed for a narrow tuning range in the cyan-blue around 495 nm, and Pr^{3+}:$LiYF_4$ (**Figure 15 d and e**) in different crystal orientations. In the latter, lasing was obtained at more than 10 emission peaks in each polarization, i.e., nearly each emission line found in the spectrum allows for lasing (cf. Figure 7). Only in the orange spectral range, Pr^{3+} suffers from $^3H_4 \rightarrow {}^1D_2$ reabsorption preventing lasing at the shortest wavelengths of

this emission band below 600 nm. It should be noted that also in the near-infrared range around 900 nm further transitions can be found which allow for broad wavelength tuning ranges.[123] These broad emission features also render Pr^{3+} very suitable for the generation of ultrashort pulses in modelocked operation mode. Utilizing Pr^{3+}-doped materials, pulses as short as 400 fs have been realized at wavelengths in the orange and red by Kerr-lens mode-locking.[83, 84, 124] Utilizing Cr^{4+}:$Y_3Al_5O_{12}$ as a modulator did not allow to overcome the Q-switched mode-locking regime, so far.[125] Q-switching was also obtained with CdSe-S glass as the saturable absorber.[14] The first demonstration of successful modelocking of Pr^{3+}:$LiYF_4$ by means of a semiconductor saturable absorber mirror (SESAM) [126] resulted in 16 mW of average output power at ~18 ps of pulse duration at 640 nm.[127] Slightly higher output power of up to 70 mW at comparable pulse duration was obtained under diode pumping with two 3.5 W diodes.[128] Further progress in the research in semiconductor modulator materials for this wavelength range may enable much shorter pulses and higher output powers in future.

3.2. Sm^{3+}-doped lasers

Laser operation in a Sm^{3+}-doped material was first demonstrated in 1979.[129] In this work, a Sm^{3+}-doped TbF_3 crystal was used as the active material in a flash-lamp pumped cryogenic laser. The high density of Tb^{3+}-ions in the crystal increased the absorption efficiency in the gain material and the population of the upper laser level $^4G_{5/2}$ was supported by energy transfer from the Tb^{3+}-ions. Later on, Ar^+-lasers emitting in the blue were utilized as pump sources for Sm^{3+}-doped materials. In this way, 10 mW of cw output power at 651 nm were obtained from a Sm^{3+}-doped glass fiber [130] and even 190 mW at ~20 % of slope efficiency were obtained from a Sm^{3+}:$LiTbF_4$ crystal emitting at 605 nm in the orange.[131] The latter material is isostructural to

$LiYF_4$ and $LiLuF_4$, but again the Tb^{3+}-ions in the host material ensured quite efficient absorption of the Ar^+-laser pump source at 488 nm with subsequent $Tb^{3+} \rightarrow Sm^{3+}$ energy transfer.

Very recently the first reports of laser operation in Sm^{3+}-doped laser materials utilizing novel semiconductor-based blue pump sources were published.[32, 132, 133]

Using a 7 mm long 1.2 at.%-doped Sm^{3+}:$LiLuF_4$-sample, nearly 100 mW of output power were obtained at slope efficiencies in the order of 15 % at 606 nm in the orange and also at 648 nm in the red spectral range under pumping with a 2ω-OPSL emitting at 479.6 nm. As predicted from the spectroscopic properties, also oxide host materials are suitable for Sm^{3+}-doped laser operation. In this case, a $SrAl_{12}O_{19}$-crystal was doped with a similar ion density of Sm^{3+}-ions compared to the $LiLuF_3$-crystal mentioned before, corresponding to a concentration of 6.8 at.% due to the different RE-site density in both materials. Furthermore, the crystal was co-doped with optically inactive Mg^{2+} on Al^{3+}-sites for charge compensation, as the Sm^{3+} occupies the divalent Sr^{2+}-site. Such a 7 mm long 6.8 at.% Sm^{3+},Mg^{2+}:$SrAl_{12}O_{19}$ crystal allowed for laser operation with nearly 50 mW of output power at 703 nm in the deep red, a transition which could not be utilized for laser operation in Sm^{3+}:$LiLuF_3$. Laser operation in the orange around 593 nm could be obtained only under chopped excitation and the slope efficiencies were as low as 1 % at output powers below 10 mW (see **Figure 16**). Laser operation around 640 nm was not observed in $SrAl_{12}O_{19}$.[32]

It should be noted that in all the laser experiments reported in [32] the laser operation showed a self-pulsing, spiking like character. Only at very low output coupler transmissions true cw operation occurred at significantly reduced efficiency in the orange with Sm^{3+}:$LiLuF_4$. The reasons for this behavior are not clear so far, but very likely the complicated energy level structure of Sm^{3+} supports detrimental processes which have not been spectroscopically revealed,

yet. Moreover, due to the low absorption cross sections the absorption efficiency of the pump remained below 25 % in all experiments. A possible improvement would be the use of GaN-based laser diodes emitting around 400 nm as pump sources, as the cross sections of this spin-allowed absorption are about one order of magnitude higher.

3.3. Tb^{3+}-doped lasers

The general suitability of Tb^{3+} for lasers in the visible spectral range was demonstrated in the 1960's.[134] Despite these early results it was regarded difficult to obtain efficient lasing in Tb^{3+}-doped materials for a long time due to the low cross sections and the risk of ESA into low lying 5d-bands. For that reason, only very few reports on successful laser experiments with Tb^{3+}-doped materials can be found. Among them are exotic experiments with very low efficiency such as lasing in a solution of terbium-trifluorocetylacetonate under flash-lamp pumping [135] or $Tb(OH)_3/SiO_2$ nanoparticles lasing at ~400 nm.[136] In fact, there is also one report on flash-lamp pumped room temperature laser operation of Tb^{3+}-doped $LiYF_4$, which was co-doped by Gd^{3+}-ions to enhance the absorption efficiency of the gain material,[137] but no further results can be found in the next decades. The first reports on blue pumping of Tb^{3+}-doped materials were published only a few years ago. A slope efficiency of 4 % was obtained from an Ar^+-laser pumped Tb^{3+}-doped fluoride fiber emitting at 543 nm.[138, 139]

Despite these not very encouraging previous results, the upcoming semiconductor-based pump sources with emission wavelengths in the blue encouraged a revisitation of several Tb^{3+}-doped fluoride crystals with respect to their laser properties. According to the absorption spectra shown in Figure 6, 2ω-OPSLs are ideally suited pump sources. Their high beam quality enables focusing with long focal lengths required in the comparably long crystals which are needed due to the low absorption cross sections. Moreover, their emission wavelengths match the absorption peak

around 485 nm. Very recently, such a pump source with a maximum output power of 4 W was successfully applied to obtain efficient laser operation in the green and yellow spectral range in a variety of Tb^{3+}-doped fluoride host materials.[40, 140] Due to the dimensions and doping concentrations of the available samples in these experiments, the absorption efficiency of the pump light was initially limited to below 30 %. With respect to the absorbed pump light, the efficiencies were much higher. Slope efficiencies of up to 55 % at a very low laser threshold of only 8 mW were realized with a 4.7 mm long 16 at.% doped Tb^{3+}:$LiYF_4$ crystal at a wavelength of 542 nm in the green. In this crystal the maximum output power was 158 mW. In contrast, a more than twice as long 14 at.% doped Tb^{3+}:$LiLuF_4$, due to its better absorption efficiency, enabled up to 613 mW of output power at 58% of slope efficiency (see **Figure 17**). Further experiments with a 21 mm long $LiLuF_4$ sample doped with as much as 28 at.% of Tb^{3+} enabled the first Tb^{3+}-doped laser with more than 1 W of output power. In this case, the optical-to-optical efficiency even with respect to the incident pump power exceeded 40%, while the slope efficiency vs. absorbed power remained as high as 52%.

Moreover, in [40] lasing of Tb^{3+} on the transition $^5D_4 \rightarrow {}^7F_4$ in the yellow spectral range was demonstrated for the first time. In this case, the slope efficiency of Tb^{3+}:$LiYF_4$ was reduced to 22 % and the highest output power with Tb^{3+}:$LiLuF_4$ was 81 mW, both at a wavelength of 587 nm (see Figure 17). These are very encouraging results considering the complicated sum-frequency mixing [141] or frequency doubling schemes [142] often applied to obtain coherent light at this wavelength. Continuous wave yellow and green laser oscillation was also observed in the host materials KY_3F_{10} and β-$BaLu_2F_8$, while Tb^{3+}:LaF_3 only allowed for a spiking self-pulsed output probably due to intraconfigurational ESA supported by the broader spectra of this material.

It should be noted that, despite the low transition cross sections of the spin-forbidden transitions in Tb^{3+}-doped materials, the output coupler transmissions were in the order of 1 % or even higher in most of these experiments. It is predicted, that even higher efficiencies can be obtained in future by the use of longer crystals with possibly even higher doping concentrations. This is supported by first successful laser experiments with stoichiometric, i.e. 100 at.% doped samples of TbF_3. Moreover, some of the crystals used in [40] did not exhibit a perfect crystal quality and no cooling was applied in the laser experiments.

3.4. Dy^{3+}-doped lasers

Despite the very low cross sections of Dy^{3+} (cf. Figure 6 and 7), this laser ion is of particular interest due to its emission in the yellow part of the spectrum. Yet it was not before 1996, when the first Dy^{3+}-doped solid state laser was realized.[143] In this case, $LiNbO_3$ served as the host material, but no further details on the pulsed output at 751 nm were presented. Also the first yellow-emitting Dy^{3+}-lasers utilizing $KY(WO_3)_2$ and $KGd(WO_3)_2$ as the host materials were operated in pulsed mode at cryogenic temperatures.[144-146] Dy^{3+}-doped glass-fibers were successfully examined for cw yellow and even blue laser operation.[147, 148] It took until 2012 when the first InGaN-diode pumped solid-state laser (Dy^{3+}:YAG) emitting in the yellow was demonstrated, but lasing was only obtained under pulsed pumping.[43]

A similar behavior was also found in Dy^{3+}:$LiLuF_4$ and Dy^{3+}:$LiYF_4$. Even under cw pumping, lasers at 578 nm (see **Figure 18**) and 574 nm operated in a self-pulsed regime [61] due to the long lifetime of the terminal laser level $^6H_{13/2}$. Co-doping with Tb^{3+}- or Eu^{3+}-ions significantly decreased the lifetime of this level and corresponding laser crystals allowed for the first cw solid state laser directly emitting in the yellow (see Figure 18).[41] The laser wavelength was shifted to 574 nm and up to now, the highest output power was 55 mW at a slope efficiency of 13 %.

Higher output powers and efficiencies at different wavelengths in the yellow seem feasible if an optimized ratio between the Dy^{3+}-ions and the co-dopant can be found. However, the occurrence of additional ESA- or cross-relaxation channels by the co-dopant cannot be excluded, as these complicated laser schemes are not fully understood, yet. Furthermore, the co-doping also enabled laser operation at 581 nm and 568 nm.[61]

3.5. Ho^{3+}-doped lasers

Due to their obvious visible fluorescence, Ho^{3+}-doped materials have attracted attention for visible lasers very early. Flash-lamp pumped laser operation at cryogenic temperatures was demonstrated at the $^5F_4, {}^5S_2 \rightarrow {}^5I_8$ transition in the green spectral range even 50 years ago in CaF_2.[149] At the $^5F_4, {}^5S_2 \rightarrow {}^5I_7$ transition around 750 nm, flash-lamp pumped pulsed laser operation was also demonstrated at room temperature in Ho^{3+}:$LiYF_4$.[150] Only recently the first report on blue-pumped laser operation of Ho^{3+} in the visible was published.[46] Laser experiments under 2ω-OPSL-pumping were conducted with Ho^{3+}:LaF_3 and Ho^{3+}:$LiLuF_3$. Even at pump power levels as high as 4 W, no laser operation could be obtained in Ho^{3+}:$LiLuF_3$ in the green and sub-mW self-pulsed output was obtained at 750 nm [132] due to the long $^5I_7$-lifetime. The output power of Ho^{3+}:LaF_3 also did not reach 10 mW at a slope efficiency of 0.4 % at 549 nm (see **Figure 19**). In both cases the laser thresholds were high. The difference between these two host materials is mainly attributed to the lower phonon energies of LaF_3 compared to $LiLuF_4$, resulting in a lower non-radiative decay rate of the emitting thermally coupled $^5F_4, {}^5S_2$-levels. Nevertheless, even in Ho^{3+}:LaF_3 the laser operation was self-pulsed, possibly due to a trapping of the non-radiatively decaying excitation in the long-living $^5I_7$-multiplet. In contrast, successful continuous wave green laser operation with 40 mW of output power was demonstrated in Ho^{3+}-doped ZBLAN fibers, which exhibit even lower phonon energies. Pumping in an

upconversion scheme at 643 nm allowed laser operation in the green around 550 nm at slope efficiencies exceeding 20 %.[151] Considering the low coupling efficiency of the pump light into the fiber and the complicated upconversion scheme, it seems likely that direct pumping in the blue spectral range enables even higher laser efficiencies in the green in Ho^{3+}:ZBLAN fibers.

3.6. Er^{3+}-doped lasers

Only few reports on directly pumped visible lasers based on Er^{3+} can be found and green laser operation of Er^{3+}-doped materials was mainly based on upconversion pumping schemes up to now.[52, 54] Nevertheless, theoretical investigations revealed, that significantly lower laser thresholds can be expected under direct pumping in the blue spectral range.[57] Previously, this approach was only followed utilizing a pulsed dye laser with pulse durations of 50 ns and a repetition rate of 10 Hz as a pump source. At an absorbed pump energy of up to 600 µJ at 486 nm, an output energy of 35 µJ at a laser wavelength of 551 nm was obtained from an Er^{3+}(1 at.%):$LiYF_4$ sample.[55] In these experiments, the slope efficiency did not exceed 6 %. Despite their significantly shorter upper state lifetimes, the laser thresholds were also reached in the oxides Er^{3+}:$Y_3Al_5O_{12}$ and Er^{3+}:$Lu_3Al_5O_{12}$.

In order to investigate the suitability of Er^{3+}-doped materials for continuous wave lasers under pumping with semiconductor-based pump sources emitting in the blue spectral range, we first performed laser experiments under InGaN-laser diode pumping at 447 nm. In this case, we succeed neither in obtaining laser operation at the maximum cw pump power of 1 W nor under quasi-cw pumping with 1.4 W of peak-power in Er^{3+}:$LiLuF_4$.

Further experiments using a 2ω-OPSL at 486.15 nm with a better beam quality and a higher output power of up to 4 W were performed. However, the pump wavelength was shifted by 0.25 nm from the absorption maximum in this spectral range. Due to the narrow absorption lines

of Er^{3+}, the effective absorption cross section was thus reduced by about a factor of four to 4×10^{-21} cm^2. Consequently, the absorption efficiency in a 2.4 mm long 1 at.% Er^{3+}-doped $LiLuF_4$ crystal amounted to only 20 %.

The laser experiments were carried out in a simple hemispherical resonator. Under strong focusing of the diffraction limited pump beam into the laser crystal with a 40-mm lens, the laser threshold was reached at absorbed pump powers of ~200 mW. Due to the off-peak pumping this corresponds to ~1 W of incident pump light. The strong focusing of the pump light resulted in thermal issues even at such comparably low pump power levels. Consequently, the highest slope efficiency of 24 % at a laser wavelength of 552 nm could be only obtained under chopped pumping (see **Figure 20**). Moreover, the output power was limited to 58 mW before a thermal roll-over of the laser curve at an absorbed pump power in the order of 0.5 W occurred. Under cw pumping, the slope efficiency was reduced to 9 % and the output power did not exceed 33 mW. Nevertheless, this is the first demonstration of direct blue semiconductor-laser pumping of visible Er^{3+}-lasers. Possibly higher absorbed pump powers can be tolerated in lower doped, longer crystals with a better distribution of the generated heat in the crystal or more sophisticated cooling schemes. Moreover, a more appropriate pump wavelength should strongly increase the absorption efficiency. In spectroscopic investigations we could not find hints for detrimental excited state absorption at the peak absorption wavelength of 486.4 nm.[60]

Due to the chopped pumping a direct comparison to the experiments performed under infrared upconversion pumping of the same crystal is difficult. The pump threshold seems to be higher under blue pumping. According to the spectroscopic investigation, no explanation for this phenomenon can be found. We attribute this to slightly different experimental conditions. Nevertheless, when compared to upconversion pumped laser experiments in a similar setup, the

absorption efficiency was higher and the slope efficiencies were decreased under blue pumping. The highest efficiencies of upconversion pumped visible Er^{3+}-lasers were obtained in a multi-pass pumping scheme, which does not allow for a precise determination of the absorbed pump power.[52] Nevertheless, the slope efficiencies with respect to the absorbed pump power are estimated to be >50 % in that setup. Therefore, we are convinced that significantly higher efficiencies than presented here are also possible under direct blue pumping.

4. Conclusion and Outlook

We reviewed the spectroscopic and laser properties of the six rare-earth ions Pr^{3+}, Sm^{3+}, Tb^{3+}, Dy^{3+}, Ho^{3+} and Er^{3+}. With all of these ions visible laser operation was obtained throughout many regions of the visible spectral range (see **Figure 21**) under pumping with novel blue-emitting semiconductor-based pump sources.

Among the rare-earth ions suitable for visible lasing, Pr^{3+} is by far the most mature. The highest efficiencies obtained with this material exceed 70 % and are comparable to those obtained with the famous Nd^{3+}-ion in the near infrared. Pr^{3+} allows for highly efficient lasing at various emission peaks in the blue, green, orange, red and deep red spectral range under pumping with InGaN-laser diodes as well as 2ω-OPSLs. Moreover, broad wavelength tuning was demonstrated around many of these peak wavelengths and initial experiments on ultrashort pulse generation were successful. Pr^{3+} has only two minor drawbacks, the first being the lack of emission peaks suitable for direct lasing in the yellow spectral range and the second being the requirement for low crystal field strengths. In the past, this limited the range of suitable host materials for efficient lasing to fluorides known for their weak thermo-mechanical properties. Nevertheless, in recent years several highly coordinated oxide host materials have been found to be suitable as

well, which gives rise to a significant further increase of the output power of Pr^{3+}-doped laser materials given the parallel evolution of suitable pump sources.

For Sm^{3+} no convincing laser results were obtained with two as contrary host materials as the oxide $SrAl_{12}O_{19}$ and the fluoride $LiLuF_4$. In both cases the lasers were prone to self-pulsing for reasons not completely understood, yet. Therefore, it is regarded difficult to find suitable host materials for efficient Sm^{3+}-lasers. Moreover, the emission wavelengths realized so far are very close to those obtained with Pr^{3+}-doped materials. Thus, Sm^{3+} is not seen as a promising laser ion for further experiments on visible laser operation in the future.

In contrast, trivalent terbium appears to be a very promising ion for the generation of visible radiation under blue pumping. If the absorption efficiency can be increased in future by the use of even higher doping concentrations and longer crystals, this ion may enable highly efficient laser operation in the green and in particular in the yellow spectral range, where most other rare-earth ions do not exhibit any fluorescence.

The same holds for trivalent dysprosium, which also allows for lasing in the yellow with even slightly shorter emission wavelengths compared to Tb^{3+}. Up to now the efficiencies are lower than those realized with Tb^{3+}-doped materials, but first investigations on co-doping quenching the lower laser level lifetime revealed that a further increase of the efficiency of yellow lasers based on Dy^{3+} can be expected.

Trivalent holmium is not regarded to be a suitable candidate for visible laser operation. Efficient cw lasers can only be expected in very low phonon energy host materials such as ZBLAN which often suffer from very undesirable chemical and thermo-mechanical properties. Moreover, the possible emission wavelengths around 550 nm and 750 nm can be obtained more efficiently with other rare earth ions such as Pr^{3+} or even Ti^{3+}:sapphire lasers.

Trivalent erbium is in fact a promising candidate for the efficient generation of green radiation under blue pumping. However, the complicated energy level scheme of Er^{3+} with the long living $^4I_{13/2}$-level always bears the risk of trapping of excitation in this level. This effect can be overcome at high pump power levels,[57] but it results in comparably high thresholds. Moreover, also in the case of erbium, the possible emission wavelengths around 550 nm are quite close to those obtained very efficiently with Pr^{3+}-doped materials.

It should be noted that for basically all of the laser systems reviewed here the conditions for optimum laser efficiency have not been found yet. Further research is required to find the perfect host materials as well as optimized growth conditions, crystal dimensions, doping concentrations, mirror transmissions and even pump-wavelengths. In particular for Tb^{3+}-doped lasers we see a possibility for a further improvement of the performance in this respect.

In general, concepts to increase the output power of bulk lasers by at least two orders of magnitude compared to the power levels reported in this review exist and their application for the lasers presented here is straightforward given the required pump power levels are available in future.

Furthermore, blue-pumped rare earth doped crystalline bulk lasers have a great potential when it comes to the generation of coherent continuous wave UV radiation by intracavity frequency doubling. Nowadays' frequency tripled and quadrupled Nd^{3+}- or Yb^{3+}-lasers are complex and expensive and often inefficient, while frequency doubling e.g. of Pr^{3+} gives access to several wavelengths in the UV with only one non-linear conversion step which can happen very efficiently inside the laser cavity. First experiments in this respect have been conducted,[66,74,113,114] but further improvement of the performance seems to be simple to obtain considering the un-optimized conditions in these first proof-of-principle experiments.

Further research in semiconductor technology will also enable significant progress in the field of SESAM-mode-locked lasers in the visible spectral range. While the Pr^{3+}-transition at 640 nm supports pulse durations in the sub-ps-range, significantly shorter pulse durations seem feasible at other transitions, e.g. in the orange, for which no suitable semiconductor absorber material exists at present. Alternatively, disordered host materials may enhance the emission bandwidth of the 640 nm transition and support even shorter pulse durations. In contrast, the long upper state lifetime of Tb^{3+} allows for an extremely large energy storage at comparably low pump power levels, which is very suitable for high-energy Q-switched pulses.

Finally, we see a variety of applications for blue-pumped rare earth doped crystalline bulk lasers in teaching and outreach. The availability of low-cost GaInN-based pump sources enables comparably cheap bulk laser systems with pump- and laser wavelengths in the visible spectral range which allows for unprecedented educational insights into basic optical and laser-physical phenomena.

Acknowledgements

This work has been supported by the graduate school 1355 “Physics with new advanced coherent light sources” and the excellence cluster “The Hamburg Centre for Ultrafast Imaging - Structure, Dynamics and Control of Matter at the Atomic Scale” of the Deutsche Forschungsgemeinschaft.

Received: ((will be filled in by the editorial staff))
Revised: ((will be filled in by the editorial staff))
Published online: ((will be filled in by the editorial staff))

Keywords: Visible lasers, rare-earth ions, solid-state lasers

References

[1] Nobel Media AB 2015, The Nobel Price in Physics 2014, *http://www.nobelprize.org/nobel_prizes/physics/laureates/2014/*, accessed November 2015.

[2] Nobel Media AB 2015, The Nobel Price in Chemistry 2014, *http://www.nobelprize.org/nobel_prizes/chemistry/laureates/2014/*, accessed November 2015.

[3] S. Nakamura, M. Senoh, S.I. Nagahama, N. Iwasa, T. Yamada, H. Kiyoku, and Y. Sugimoto, *Jpn. J. Appl. Phys.* **35**, L74-L76 (1996).

[4] Swiss National Centre of Competence in Research Molecular Ultrafast Science and Technology (NCCR MUST), Exhibition and teaching laser program, http://www.nccr-must.ch/year_of_light/exhibition_and_teaching_laser_program.html, accessed November 2015.

[5] L. McDonagh and R. Wallenstein, *Opt. Lett.* **32**, 802-804 (2007).

[6] T. Meier, B. Willke, and K. Danzmann, *Opt. Lett.* **35**, 22, 3742-3744 (2010).

[7] J.P. Negel, A. Loescher, A. Voss, D. Bauer, D.H. Sutter, A. Killi, M.A. Ahmed, and T. Graf, *Proc. SPIE*, San Francisco, USA, talk 9342 (2015).

[8] G.H. Dieke, Spectra and Energy Levels of Rare Earth Ions in Crystals. Wiley Interscience, New York (1968).

[9] P.S. Peijzel, A. Meijerink, R.T. Wegh, M.F. Reid, and G.W. Burdick, *J. Solid State Chem.* **178**, 448-453 (2005).

[10] M. Kuznetsov, F. Hakimi, R. Sprague, and A. Mooradian, *IEEE Photon. Technol. Lett.* **9**, 1063-1065 (1997).

[11] J.G. McInerney, A. Mooradian, A. Lewis, A.V. Shchegrov, E.M. Strzelecka, D. Lee, J.P. Watson, M. Liebman, G.P. Carey, B.D. Cantos, W.R. Hitchens, and D. Heald, *Electron. Lett.* **39**, 523-525 (2003).

[12] Coherent, Inc., Product Page Genesis Taipan, http://www.coherent.com/Products/?1891/Genesis-Taipan-460-nm-to-577-nm, accessed November 2015.

[13] A. Tyagi, Y.D. Lin, D.A. Cohen, M. Saito, K. Fujito, J.S. Speck, S.P. DenBaars, and S. Nakamura, *Appl. Phys. Express* **1**, 091103-1-3 (2008).

[14] K. Iijima, R. Kariyama, H. Tanaka, K. Hirosawa, and F. Kannari, *ECLEO*, Munich, Germany, talk CA-8.1-TUE (2015).

[15] S. Nakamura, S. Pearton, and G. Fasol, "The Blue Laser Diode", Springer Science & Business Media (2014).

[16] D.T. Marzahl, F. Reichert, P.W. Metz, M. Fechner, N.O. Hansen, and G. Huber, *Appl. Phys. B* **116**, 109-113 (2014).

[17] J.G. Mcinerney, A. Mooradian, A. Lewis, A.V. Shchegrov, E.M. Strzelecka, D. Lee, J.P. Watson, M.K. Liebmann, G.P. Carey, A. Umbrasas, C.A. Amsden, B.D. Cantos, W.R. Hitchens, D.L. Heald, V.V. Doan, and J.L. Cannon, *Proc. SPIE,* San Francisco, USA, 4942, 1 (2003).

[18] Nichia Corporation, Laserdiodes, *http://www.nichia.co.jp/de/product/laser.html*, accessed November 2015.

[19] R.M. Macfarlane, F. Tong, A.J. Silversmith, and W. Lenth , *Appl. Phys. Lett.* **52**, 1300-1302 (1988).

[20] V.I. Dashkevich, S.N. Bagayev, V.A. Orlovich, A.A. Bui, A.A. Loiko, K.V. Yumashev, N.V. Kuleshov, S.M. Vatnik, and A.A. Pavlyuk, *Laser Phys. Lett.* **12**, 015006 (6pp) (2015).

[21] T. Hebert, R. Wannemacher, R.M. Macfarlane, and W. Lenth, *Appl. Phys. Lett.* **60**, 2592-2594 (1992).

[22] N.P. Barnes, B.M. Walsh, and D.J. Reichley, *ASSL*, San Diego, USA, talk AT4A.24 (2012).

[23] M. Malinowski, M.F. Joubert, R. Mahiou, and B. Jacquier, *J. Phys. IV France* 04, C4-541 (1994).

[24] H.W. Moos, *J. Lumin.* **1-2**, 106-121 (1970).

[25] P. Dorenbos, *J. Lumin.* **91**, 155-176 (2000).

[26] P. Dorenbos, *Phys. Rev. B* **62**, 15640-15648 (2000).

[27] M. Laroche, A. Braud, S. Girard, J. L. Doualan, R. Moncorgé, and M. Thuau, J. Opt. Soc. Am. B 16, 2269-2277 (1999) .

[28] M. Laroche, J. L. Doualan, S. Girard, J. Margerie, and R. Moncorgé, J. Opt. Soc. Am. B 17, 1291-1303 (2000).

[29] M. Fibrich, H. Jelinkova, J. Sulc, K. Nejezchleb, and V. Skoda, *Las. Phys. Lett.* **8**, 559-568 (2011).

[30] G.Q. Wang, X.H. Gong, Y.F. Lin, Y.J. Chen, J.H. Huang, Z.D. Luo, and Y.D. Huang, *Opt. Mater.* **37**, 229-234 (2014).

[31] S. Duffy, J.P.R. Wells, H.H. Gallagher, and T.P.J. Han, *J. Cryst. Growth* **203**, 405-411 (1999).

[32] D.T. Marzahl, P.W. Metz, C. Kränkel, and G. Huber, *Opt. Express* **23**, 21118-2127 (2015)

[33] M. Yamada, H. Uno, S.I. Tsuda, J.P.R. Wells, and T.P.J. Han, *J. Lumin.* **132**, 16081617 (2012).

[34] A. Lupei, V. Lupei, and C. Gheorghe, *Opt. Mat.* **36**, 419-424 (2013).

[35] H.P. Christensen, *Phys. Rev. B* **17**, 4060-4068 (1978).

[36] V. Vasyliev, E.G. Villora, Y. Sugahara, and K. Shimamura, *J. Appl. Phys.* **113**, 203508-1-9 (2013).

[37] R. Moncorgé, J. Margerie, J. L. Doualan, P. Nagtegaele, Y. Guyot, and M. F. Joubert, J. Phys. IV France 138, 171-179 (2006).

[38] J. L. Ryan and C. K. Jørgensen, J. Phys. Chem. 70, 2845-2857 (1966).

[39] L. van Pieterson, M. F. Reid, G. W. Burdick, and A. Meijerink, Phys. Rev. B. 65, 045114 (2002).

[40] P.W. Metz, D.T. Marzahl, A. Majid, C. Kränkel, and G. Huber, *Las. Photonics Rev.* published online, *http://dx.doi.org/10.1002/lpor.201500274* (2015).

[41] G. Bolognesi, D. Parisi, D. Calonico, G.A. Constanzo, F. Levi, P.W. Metz, C. Kränkel, G. Huber, and M. Tonelli, *Opt. Lett.* **39**, 6628-6631 (2014).

[42] S. Bigotta, M. Tonelli, E. Cavalli, and A. Belletti, *J. Lumin.* **130**, 13-17 (2010).

[43] S.R. Bowman, S. O'Connor, and N.J. Condon, *Opt. Express* **20**, 12906-12911 (2012).

[44] P. Koopmann, S. Lamrini, K. Scholle, M. Schäfer, P. Fuhrberg, and G. Huber, *Opt. Express* **21**, 3926-3931 (2013).

[45] B.M. Walsh, G.G. Grew, and N.P. Barnes, *J. Phys. - Condens. Mat.* **17**, 7643-7665 (2005).

[46] F. Reichert, F. Moglia, P.W. Metz, A. Arcangeli, D.T. Marzahl, S. Veronesi, D. Parisi, M. Fechner, M. Tonelli, and G. Huber, *Opt. Express* **5**, 88-101 (2014).

[47] M.C. Nostrand, R.H. Page, S.A. Payne, L.I. Isaenko, and A.P. Yelisseyev, *J. Opt. Soc. Am. B* **18**, 264-276 (2001).

[48] K. Rademaker, W.F. Krupke, R.H. Page, S.A. Payne, K. Petermann, G. Huber, A.P. Yelisseyev, L.I. Isaenko, U.N. Roy, A. Burger, K.C. Mandal, and K. Nitsch, *J. Opt. Soc. Am. B* **21**, 2117-2129 (2004).

[49] D. Garbuzov, I. Kudryashov, and M. Dubinskii, *Appl. Phys. Lett.* **87**, 121101 (2005).

[50] T. Li, K. Beil, C. Kränkel, and G. Huber, *Opt. Lett.* **37**, 2568-2570 (2012).

[51] T. Jensen, A. Diening, G. Huber, and B.H.T. Chai, *Opt. Lett.* **21**, 585-587 (1996).

[52] F. Moglia, S. Müller, F. Reichert, P.W. Metz, T. Calmano, C. Kränkel, E. Heumann, and G. Huber, *Opt. Mater.* **42**, 167-173 (2015).

[53] L.F. Johnson and H.J. Guggenheim, Appl. Phys. Lett. **19**, 44 (1971).

[54] T. Danger, J. Koetke, R. Brede, E. Heumann, G. Huber, and B.H.T. Chai, *J. Appl. Phys.* **76**, 1413-1422 (1994).

[55] R. Brede, T. Danger, E. Heumann, G. Huber, and B.H.T. Chai, *Appl. Phys. Lett.* **63**, 729-730 (1993).

[56] S. Bjurshagen, J.E. Hellström, V. Pasiskevicius, M.C. Pujol, M. Aguilo, and F. Diaz, *Appl. Opt.* **45**, 4715-4725 (2006).

[57] O. Toma, *IEEE J. Quantum Electron.* **43**, 519-526 (2007).

[58] N.O. Hansen, *PhD Thesis*, Universität Hamburg, Germany (2011).

[59] F. Reichert, *PhD Thesis*, Universität Hamburg, Germany (2013).

[60] F. Moglia, *PhD Thesis*, Universität Hamburg, Germany (2013).

[61] P.W. Metz, *PhD Thesis*, Universität Hamburg, Germany (2014).

[62] M.J. Weber, Handbook of Optical Materials, Boca Raton, London, Washington DC, CRC Press (2003).

[63] R.E. Thoma, C.F.F. Weaver, H. A., H. Insley, L.A. Harris, and H.A. Yakel Jr., *J. Phys. Chem.* **65**, 1096-1099 (1961).

[64] D. Maier, R. Bertram, D. Klimm, and R. Fornari, *Cryst. Res. Technol.* **44**, 137-140 (2009).

[65] R.E. Thoma, G.D. Brunton, R.A. Penneman, and T.K. Keenan, *Inorg. Chem.* **9**, 1096-1101 (1970).

[66] A. Richter, E. Heumann, G. Huber, V.G. Ostroumov, and W. Seelert, *Opt. Express* **15**, 5172-5178 (2007).

[67] B. Xu, P. Camy, J.L. Doualan, Z. Chai, and R. Moncorgé, *Opt. Express* **19**, 1191-1197 (2011).

[68] R. G. Smart, J. N. Carter, A. C. Tropper, D. C. Hanna, S. T. Davey, S. F. Carter, and D. Szebesta, Opt. Commun. 86, 337-340 (1991).

[69] A. Richter, H. Scheife, E. Heumann, and G. Huber, Electron. Lett. 41, 794-795 (2005).

[70] H. Okamoto, K. Kasuga, I. Hara, and Y. Kubota, Opt. Express 17, 20227-20232 (2009)

[71] Y. Fujimoto, J. Nakanishi, T. Yamada, O. Ishii, and M. Yamazaki, Prog. Quant. Electron. 37, 185-214 (2013).

[72] P.W. Metz, K. Hasse, D. Parisi, N.O. Hansen, C. Kränkel, M. Tonelli, and G. Huber, *Opt. Lett.* **39**, 5158-5161 (2014).

[73] P.W. Metz, F. Reichert, F. Moglia, S. Mueller, D.T. Marzahl, C. Kränkel, and G. Huber, *Opt. Lett.* **39**, 3193-3196 (2014).

[74] V.G. Ostroumov and W. Seelert, *Proc. SPIE*, talk 6871 (2008).

[75] T. Gün, P.W. Metz, and G. Huber, *Opt. Lett.* **36**, 1002-1004 (2011).

[76] B. Qu, S.Y. Luo, Y.J. Cheng, H.Y. Xu, Z.P. Cai, P. Camy, J.L. Doualan, and R. Moncorgé, *IEEE Photon. Technol. Lett.* **27**, 333-335 (2015).

[77] Z.L. Liu, Z.P. Cai, S.L. Huang, C.H. Zeng, Z.Y. Meng, Y.K. Bu, Z.Q. Luo, B. Xu, H.Y. Xu, C.C. Ye, F. Stareki, P. Camy, and R. Moncorgé, *J. Opt. Soc. Am. B* **30**, 302-305 (2013).

[78] A. Yariv, *J. Appl. Phys.* **33**, 2519-2520 (1962).

[79] R. Solomon and M. Mueller, *Appl. Phys. Lett.* **3**, 135-137 (1963).

[80] F. Varsanyi, *Appl. Phys. Lett.* **19**, 169-171 (1971).

[81] L. Esterowitz, R. Allen, M. Kruer, F. Bartoli, and L.S. Goldberg, *J. Appl. Phys.* **48**, 650-652 (1977).

[82] T. Sandrock, T. Danger, E. Heumann, G. Huber, and B.H.T. Chai, *Appl. Phys. B* **58**, 149-151 (1994).

[83] S. Ruan, J.M. Sutherland, P.M.W. French, J.R. Taylor, and B.H.T. Chai, *Opt. Lett.* **20**, 1041-1043 (1995).

[84] J.M. Sutherland, P.M. French, J.R. Taylor, and B.H.T. Chai, *Opt. Lett.* **21**, 797-799 (1996).

[85] F. Cornacchia, A. Richter, E. Heumann, G. Huber, D. Parisi, and M. Tonelli, *Opt. Express* **16**, 992-1002 (2007).

[86] P. Camy, J.L. Doualan, R. Moncorgé, J. Bengoechea, and U. Weichmann, *Opt. Lett.* **32**, 1462-1464 (2007).

[87] A. Richter, N. Pavel, E. Heumann, G. Huber, D. Parisi, A. Toncelli, M. Tonelli, A. Diening, and W. Seelert, *Opt. Express* **14**, 3282-3287 (2006).

[88] D. Paboeuf, O. Mhibik, F. Bretenaker, P. Goldner, D. Parisi, and M. Tonelli, *Opt. Lett.* **36**, 280-282 (2011).

[89] A. Sottile, D. Parisi, and M. Tonelli, *Opt. Express* **22**, 13784-13791 (2014).

[90] T.T. Basiev, V.A. Konyushkin, D.V. Konyushkin, M.E. Doroshenko, G. Huber, F. Reichert, N.O. Hansen, and M. Fechner, *Opt. Mater. Express* **1**, 1511-1514 (2011).

[91] F. Reichert, F. Moglia, D.T. Marzahl, P. Metz, M. Fechner, N.O. Hansen, and G. Huber, *Opt. Express* **20**, 20387-20395 (2012).

[92] P.W. Metz, D.T. Marzahl, F. Reichert, C. Kränkel, and G. Huber, *EPS-QEOD Europhoton Conference*, Neuchâtel, Switzerland, poster ThP-T1-P-22 (2014).

[93] P.W. Metz, D.T. Marzahl, C. Guguschev, R. Bertram, C. Kränkel, and G. Huber, *Opt. Lett.* **40**, 2699-2702 (2015).

[94] T. Danger, A. Bleckmann, and G. Huber, *Appl. Phys. B* **58**, 413-420 (1994).

[95] M. Fibrich, H. Jelinkova, J. Sulc, K. Nejezchleb, and V. Skoda, *Appl. Phys. B* **97**, 363-367 (2009).

[96] M. Fechner, A. Richter, N.O. Hansen, A.G. Petrosyan, K. Petermann, and G. Huber, *ECLEO*, Munich, Germany, talk CA-6.3 Tue (2009).

[97] L.D. Merkle, B. Zandi, R. Moncorgé, Y. Guyot, R. Verdun, and H.B. McIntosh, *J. Appl. Phys.* **79**, 1849-1856 (1996).

[98] M. Fechner, F. Reichert, N.O. Hansen, K. Petermann, and G. Huber, *Appl. Phys. B* **102**, 731-735 (2011).

[99] D.T. Marzahl, F. Reichert, M. Fechner, N.O. Hansen, K. Petermann, and G. Huber, *EPS-QEOD Europhoton Conference*, Stockholm, Sweden, talk ThP.3 (2012).

[100] H.S. Yoder and M.L. Keith, *J. Min. Soc. Am.* **36**, 7&8, 519-533 (1950).

[101] C. Kränkel, *IEEE J. Sel. Top. Quant. Electron.* **21**, 1602013 (2015).

[102] A. Richter, E. Heumann, E. Osiac, G. Huber, W. Seelert, and A. Diening, *Opt. Lett.* **29**, 2638-2640 (2004).

[103] T. Calmano, J. Siebenmorgen, F. Reichert, M. Fechner, A.G. Paschke, N.O. Hansen, K. Petermann, and G. Huber, *Opt. Lett.* **36**, 4620-4622 (2011).

[104] S. Müller, T. Calmano, P.W. Metz, N.O. Hansen, C. Kränkel, and G. Huber, *Opt. Lett.* **37**, 5223-5225 (2012).

[105] A. Voss, F. Reichert, P.W. Metz, D.T. Marzahl, C. Kränkel, G. Huber, and T. Graf, *Opt. Lett.* **39**, 1322-1325 (2014).

[106] E. Osiac, E. Heumann, A. Richter, G. Huber, A. Diening, and W. Seelert, *CLEO*, San Francisco, USA, talk CFE2 (2004).

[107] F. Reichert, D.T. Marzahl, P. Metz, M. Fechner, N.O. Hansen, and G. Huber, *Opt. Lett.* **37**, 4489-4891 (2012).

[108] F. Reichert, T. Calmano, S. Müller, D.T. Marzahl, P.W. Metz, and G. Huber, *Opt. Lett.* **38**, 2698-2701 (2013).

[109] F. Stareki, W. Bolanos, A. Braud, J.L. Doualan, G. Brasse, A. Benayad, V. Nazabal, B. Xu, R. Moncorgé, and P. Camy, *Opt. Lett.* **38**, 455-457 (2013).

[110] W. Bolanos, G. Brasse, F. Stareki, A. Braud, J.L. Doualan, R. Moncorge, and P. Camy, *Opt. Lett.* **39**, 4450-4453 (2014).

[111] M. Malinowski, M.F. Joubert, and B. Jacquier, *Phys. Stat. Sol. (a)* **140**, K49-K52 (1993).

[112] P.W. Metz, D. Parisi, K. Hasse, N.O. Hansen, C. Kränkel, M. Tonelli, and G. Huber, *ASSL*, Paris, France, talk AF2A.7 (2013).

[113] V.G. Ostroumov, W. Seelert, L. Hunziker, C. Ihli, A. Richter, E. Heumann, and G. Huber, *Proc. SPIE,* San Francisco, USA, talk 6451 (2007).

[114] T. Gün, P. Metz, and G. Huber, *Appl. Phys. Lett.* **99**, 181103 (2011).

[115] J. Lehmann, P. Metz, T. Gün, and G. Huber, DFG Frühjahrstagung, Stuttgart, Germany, talk Q 18.10 (2012).

[116] Z.K. Liu, Z.P. Cai, X. Bin, C.H. Zheng, S.L. Hung, F.J. Wang, Y.L. Yan, and H.Y. Xu, *IEEE Photon. J.* **5**, 1500905 (2013).

[117] A. Richter, *PhD Thesis*, Universität Hamburg, Germany (2008).

[118] Y. Dong, S.T. Li, and X.H. Zang, *Las. Phys. Lett.* **9**, 116-119 (2012).

[119] M. Fibrich and H. Jelinkova, *Las. Phys. Lett.* **10**, 105814 (2013).

[120] B. Xu, F. Stareki, D. Paboeuf, P. Camy, J.L. Doualan, Z.P. Cai, A. Braud, R. Moncorgé, P. Goldner, and F. Bretenaker, *Opt. Express* **21**, 5567-5574 (2013).

[121] P.W. Metz, S. Mueller, F. Reichert, D.T. Marzahl, F. Moglia, C. Kränkel, and G. Huber, *Opt. Express* **21**, 31274-31281 (2013).

[122] G.B. Venus, A. Sevian, V.I. Smirnov, and L.B. Glebov, *Conference on High-Power Diode Laser Technology and Applications III*, San Jose, USA, talk 166-176 (2005).

[123] B. Qu, R. Moncorgé, Z. Cai, J.L. Doualan, B. Xu, A. Braud, and P. Camy, *Opt. Lett.* **40**, 13, 3053-3056 (2015).

[124] Y.P. Tong, J.M. Sutherland, P.M.W. French, J.R. Taylor, A.V. Shestakov, and B.H.T. Chai, *Opt. Lett.* **21**, 644-646 (1996).

[125] R. Abe, J. Kojou, K. Masuda, and F. Kannari, *Appl. Phys. Express* **6**, 032703-1-4 (2013).

[126] U. Keller, *Nature* **424**, 831-838 (2003).

[127] M. Gaponenko, P.W. Metz, A. Härkönen, A. Heuer, T. Leinonen, M. Guina, T. Südmeyer, G. Huber, and C. Kränkel, *Opt. Lett.* **39**, 6628-6631 (2014).

[128] R. Kariyama, H. Tanaka, K. Iijima, K. Hirosawa, and F. Kannari, *ECLEO*, Munich, Germany, poster CA-P.23-SUN (2015).

[129] B.N. Kazakov, M.S. Orolov, M.V. Petrov, A.L. Stolov, and A.M. Tkachuk, *Opt. Spectrosc.* **47**, 676-677 (1979).

[130] M.C. Farries, P.R. Morkel, and J.E. Townsend, *Electron. Lett.* **24**, 709-711 (1988).

[131] H.P. Jenssen, *ASSL*, Memphis, USA, talk ME2-1 (1995).

[132] C. Kränkel, P.W. Metz, F. Reichert, F. Moglia, D.T. Marzahl, and G. Huber, *ASSL*, Shanghai, China, talk ATu3A.4 (2014).

[133] D.T. Marzahl, F. Reichert, B. Stumpf, P.W. Metz, C. Kränkel, and G. Huber, *CLEO*, San Jose, USA, talk STu2F.4 (2014).

[134] S.I. Andreev, M.R. Bedilov, G.O. Karapatyan, and V.M. Likhachev, *Sov. J. Opt. Tech.* **34**, 819 (1967).

[135] S. Bjorklund, G. Kellermeyer, C.R. Hurt, N. MacAvoy, and N. Filipescu, *Appl. Phys. Lett.* **10**, 160-162 (1967).

[136] H.Y. Lin, H.K. Fu, C.L.C. Cheng, Y. F., Y.S. Lin, Y. Hung, and C.Y. Mou, *Opt. Express* **16**, 16697-16703 (2008).

[137] H.P. Jenssen, D. Castleberry, D.R. Gabbe, and A. Linz, *IEEE J. Quantum Electron.* **9**, 665-665 (1973).

[138] T. Yamashita and Y. Oshishi, *Jpn. J. Appl. Phys.* **46**, L991 (2007).

[139] T. Yamashita, G. Qin, T. Suzuki, and Y. Ohishi, *OFC and NFOE Conference*, San Diego, USA, poster JWA18 (2008).

[140] P.W. Metz, C. Kränkel, and G. Huber, *EPS-QEOD Europhoton Conference*, Neuchâtel, Switzerland, talk FrB-T1-O-07 (2014).

[141] Y. Chen and S. Tsai, *Opt. Lett.* **27**, 397-399 (2002).

[142] C.B. Olausson, A. Shirakawa, M. Chen, J.K. Lyngsø, J. Broeng, K.P. Hansen, A. Bjarklev, and K. Ueda, *Opt. Express* **18**, 16345-16352 (2010).

[143] M. Malinowski, P. Myziak, R. Piramidowicz, I. Pracka, T. Lukasiewicz, B. Surma, S. Kaczmarek, K. Kopcynski, and Z. Mierczyk, *Acta Phys. Pol.* **90**, 181-189 (1996).

[144] A.A. Kaminskii, U. Hömmerich, D. Temple, J.T. Seo, and A.A. Pavlyuk, *Phys. Stat. Sol. (a)* **174**, R7 (1999).

[145] A.A. Kaminskii, J.B. Gruber, S.N. Bagaev, K.I. Ueda, U. Hömmerich, J.T. Seo, D. Temple, B. Zandi, A.A. Korneienko, A.A. Dunina, E.B. Pavlyuk, R.F. Klevtsova, and F.A. Kuznetsov, *Phys. Rev. B* **65**, 125108-1-29 (2003).

[146] A.A. Kaminskii, *Phys. Stat. Sol. (a)* **200**, 215-296 (2003).

[147] J. Limpert, H. Zellmer, P. Riedel, G. Maze, and A. Tünnermann, *Electron. Lett.* **36**, 1386-1387 (2000).

[148] Y. Fujimoto, O. Ishii, and M. Yamazaki, *Electron. Lett.* **46**, 586-587 (2010).

[149] Y.K. Voronko, A.A. Kaminskii, V.V. Osiko, and A.M. Prokhorov, *JETP Lett.* **1**, 3 (1965).

[150] E.P. Chicklis, C. Naiman, L. Esterowitz, and R. Allen, *IEEE J. Quant. Electron.* **13**, 980-992 (1977).

[151] D.S. Funk and J.G. Eden, *IEEE J. Quant. Electron.* **37,** 980-992 (2001).

Figures

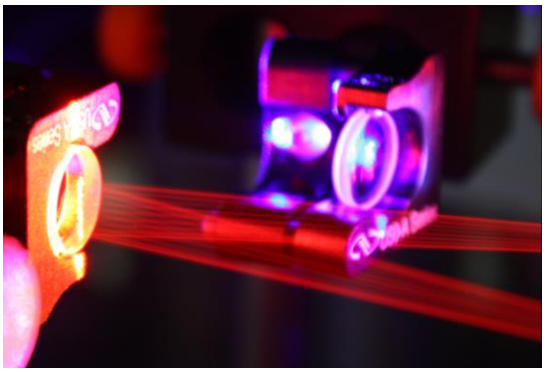

Figure 1: Detail of a blue-pumped, red emitting solid state laser resonator (Pr^{3+}:$LiYF_4$) intentionally misaligned to demonstrate high order transversal mode operation.

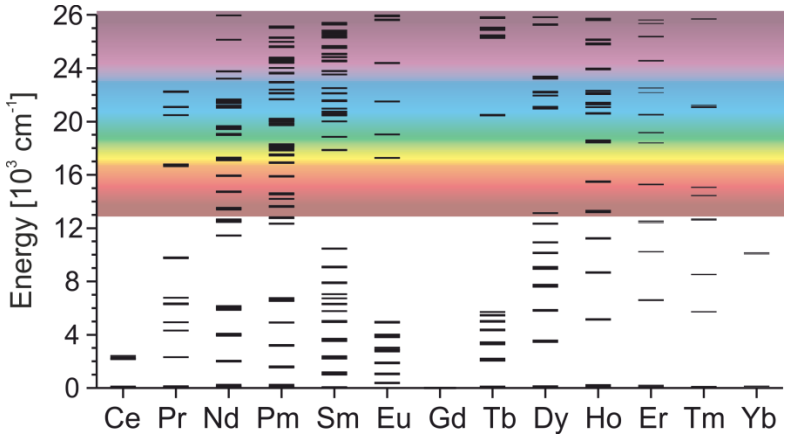

Figure 2. Energetic position of the energy levels of rare-earth ions in $LaCl_3$ (after [8, 9]).

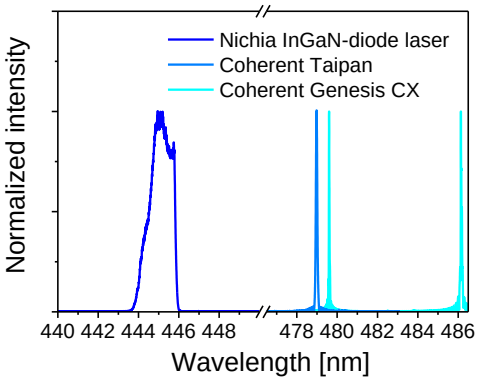

Figure 3: Typical emission spectra of an InGaN-based diode laser at 445 nm and three different 2ω-OPSLs emitting at distinct wavelengths around 480 nm.

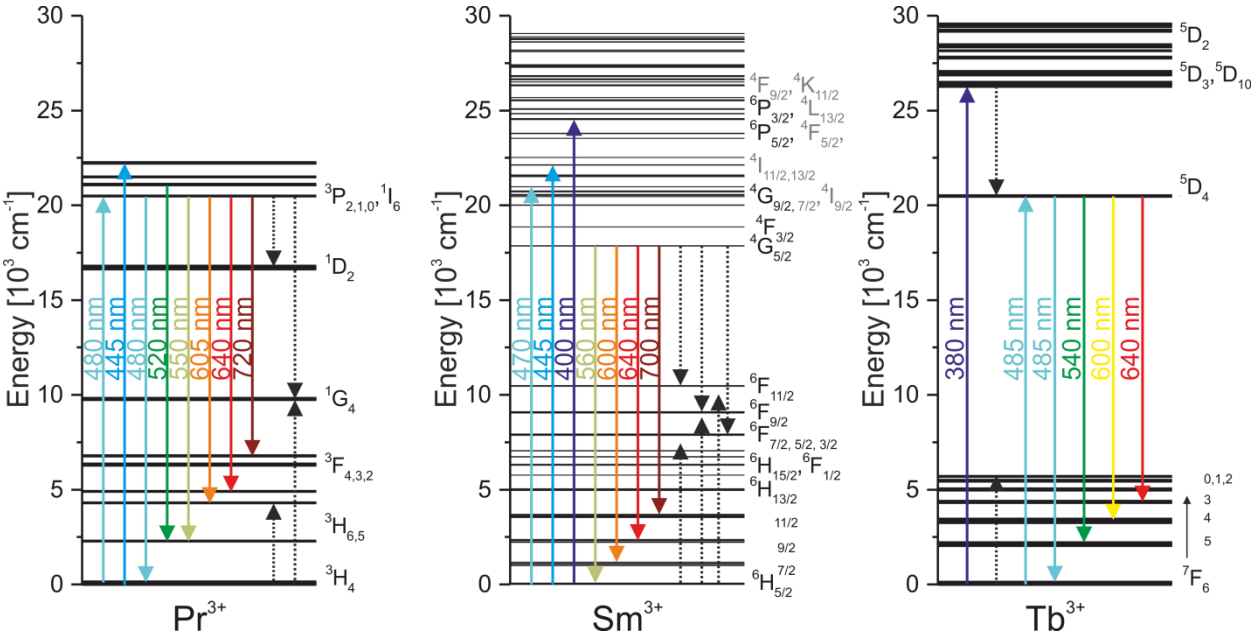

Figure 4: Energy level scheme of the lowest energy levels of the $4f^n$-configuration of Pr^{3+}, Sm^{3+} and Tb^{3+} with corresponding absorption and emission transitions in the visible (solid arrows) and possible cross-relaxation channels (dotted arrows). For clarity, some of the less important levels are labelled in lighter grey in the Sm^{3+}-scheme.

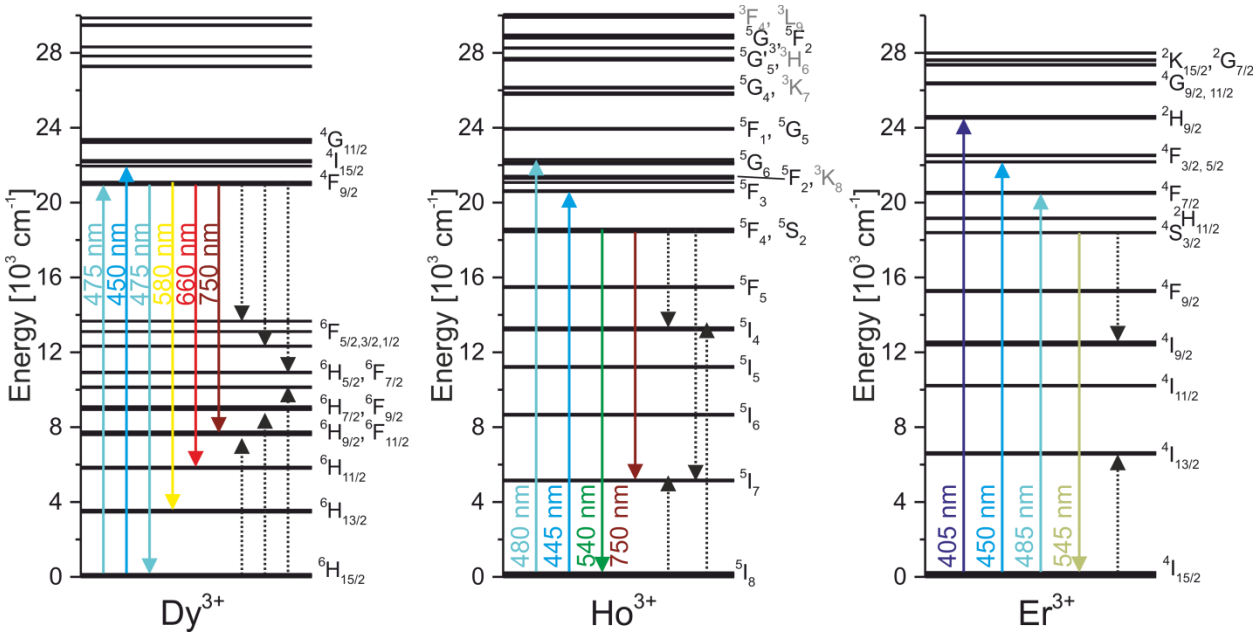

Figure 5: Energy level scheme of the lowest energy levels of the $4f^n$-configuration of Dy^{3+}, Ho^{3+} and Er^{3+} with corresponding absorption and emission transitions in the visible (solid arrows) and possible cross-relaxation channels (dotted arrows). For clarity, some of the less important levels are labelled in lighter grey in the Ho^{3+}-scheme.

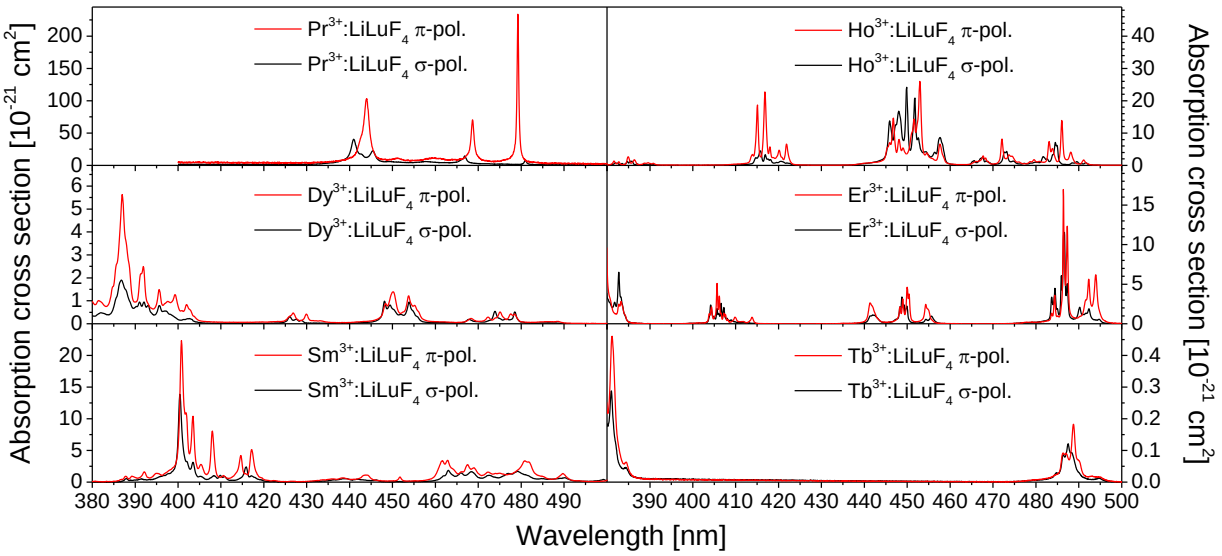

Figure 6. Polarized absorption cross section spectra in the blue part of the visible range of $LiLuF_4$ doped with different rare-earth ions.[58-61]

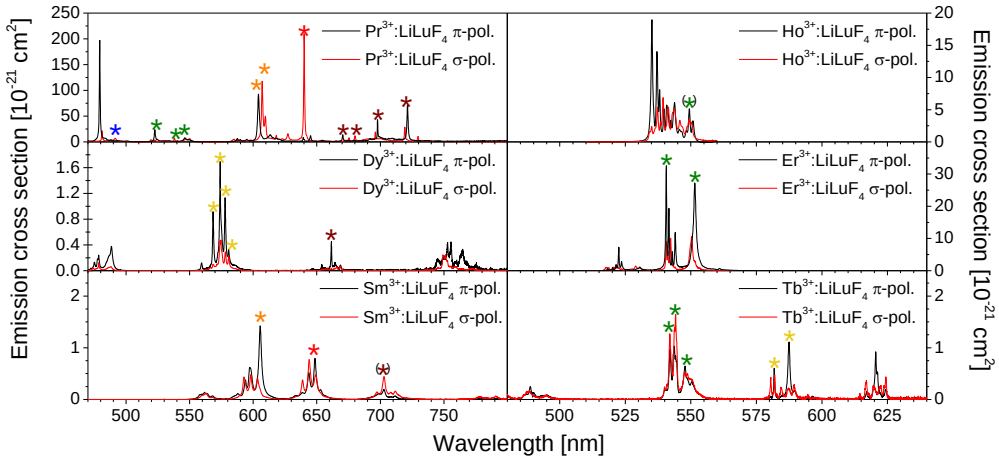

Figure 7. Polarized emission cross section spectra in the visible spectral range of $LiLuF_4$ doped with different rare-earth ions. The stars mark transitions on which laser operation was obtained under blue semiconductor laser pumping and the respective color. Brackets indicate transitions on which lasing was obtained only in other hosts. Please note that broad tuning can be obtained around some of these transitions.[58-61]

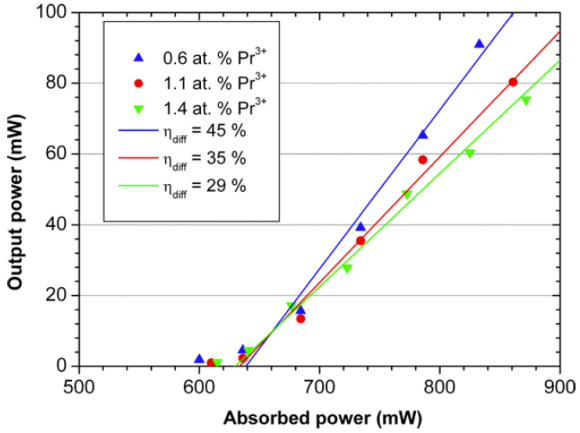

Figure 8: Output characteristics of InGaN-laser diode pumped Pr^{3+}:$YAlO_3$ at 747 nm (with permission of Ref. [95]. Copyright 2009 Springer Berlin Heidelberg).

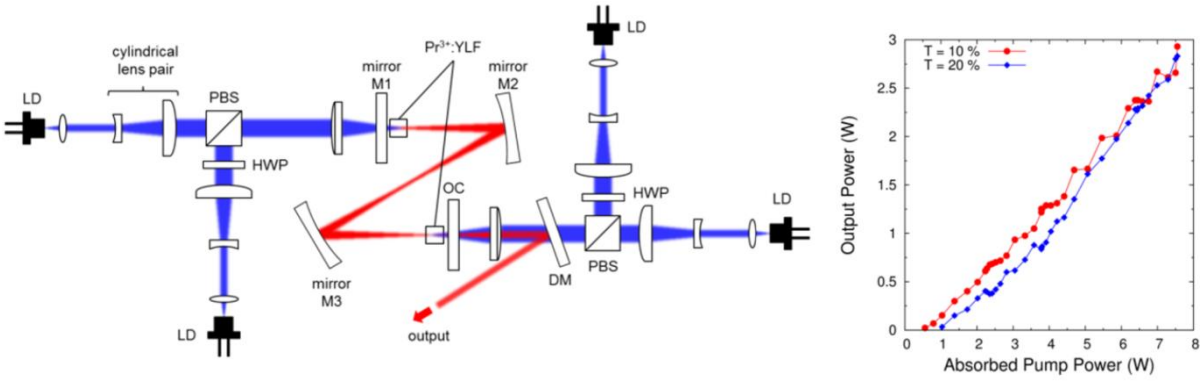

Figure 9: (left) Pr^{3+}:YLF laser pumped by four blue InGaN-laser diodes (LD). (right) Output characteristics in cw operation at 640 nm with two different output coupler transmissions (with permission of Ref. [14] . Copyright 2014 European Physical Society).

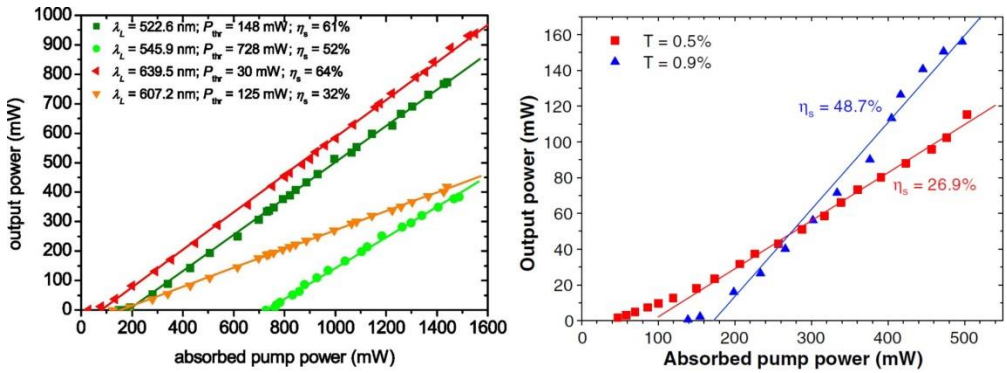

Figure 10: (left): Output characteristics of Pr^{3+}:YLF pumped by two blue InGaN-laser diodes in cw operation at 4 wavelengths between 522.6 nm and 639.5 nm (with permission of Ref. [75]. Copyright 2011 Optical Society of America). (right): Output characteristics of Pr^{3+}:YLF pumped by one blue InGaN-laser diode in cw operation at 698 nm (with permission of Ref. [77]. Copyright 2013 Optical Society of America).

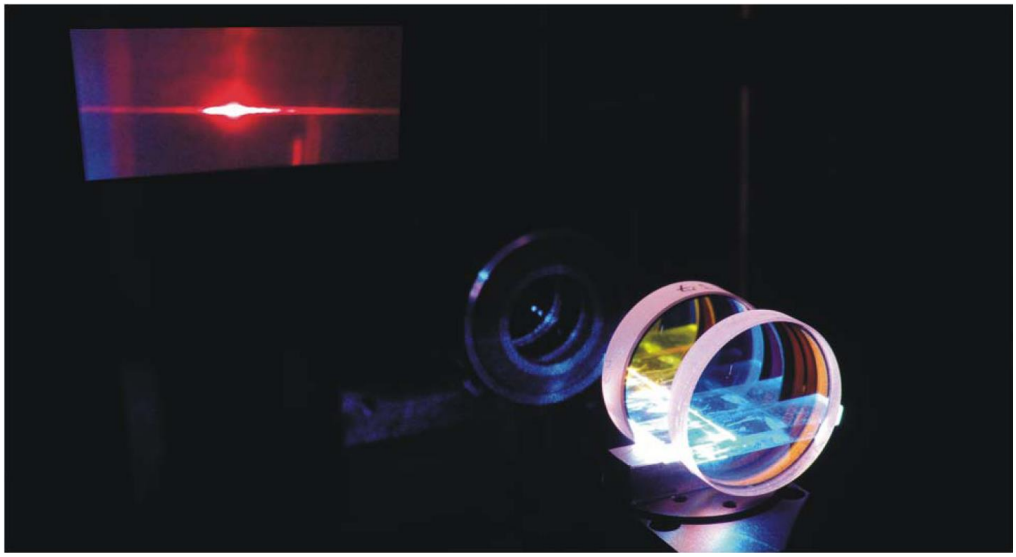

Figure 11: Photograph of an epitaxial $LiY_{0.035}Gd_{0.05}Pr_{0.015}F_4$ planar waveguide laser setup during laser operation (with permission of Ref. [109]. Copyright 2014 Optical Society of America).

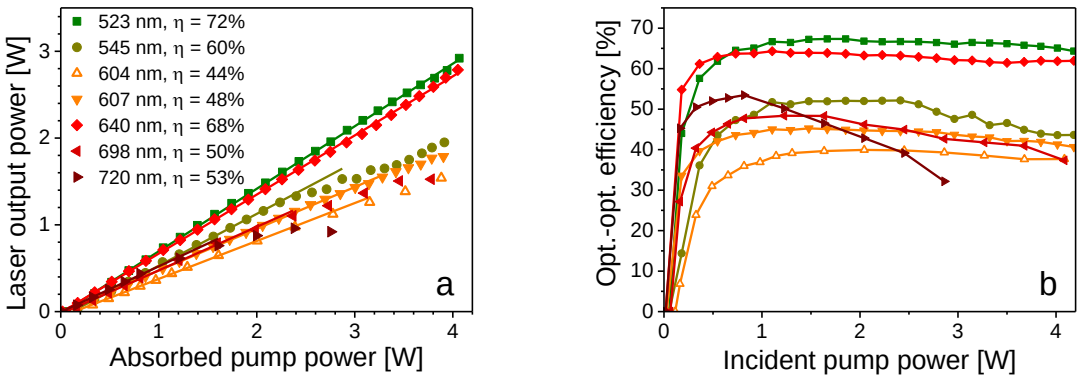

Figure 12: Laser characteristics (a) and optical-to-optical efficiencies (b) of 2ω-OPSL-pumped Pr^{3+}:$LiYF_4$ lasers at different laser emission wavelengths.[73]

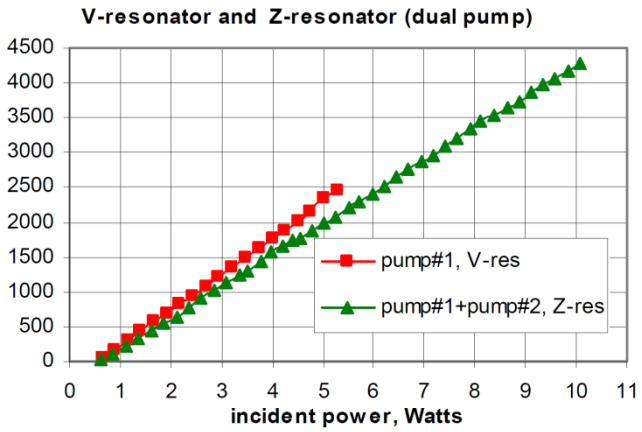

Figure 13: Laser characteristics of a Pr^{3+}:$LiYF_4$ laser under pumping with one (red curve) and two (green curve) 2ω-OPSLs at 479 nm. The slope efficiency was 45 % with respect to the incident pump power in these experiments. From [74], copyright SPIE, the international society for optics and photonics. Reproduced with permission.

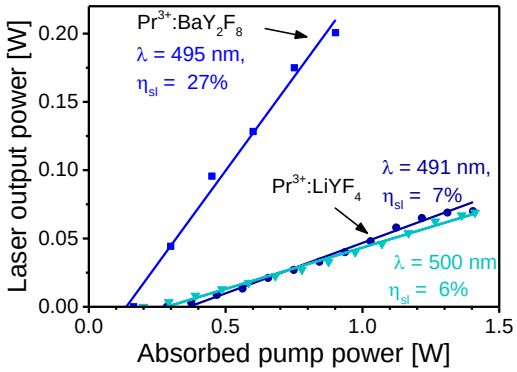

Figure 14: Laser characteristics of 2ω-OPSL-pumped cyan-blue-emitting Pr^{3+}-lasers.[72]

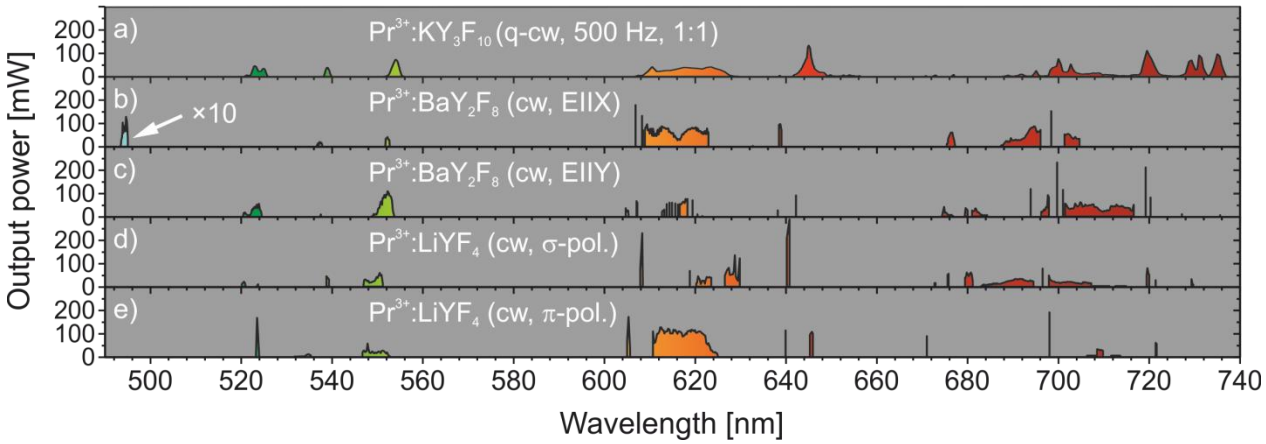

Figure 15: Wavelength tuning ranges of different Pr^{3+}-doped fluoride crystals in different crystallographic orientations. A birefringent quartz filter was used as a wavelength selective element and a 1-W InGaN-laser diode at 444 nm served as the pump source. For clarity, the tuning curve of Pr^{3+}:BaY_2F_8 was enhanced by a factor of 10 at wavelengths below 500 nm.

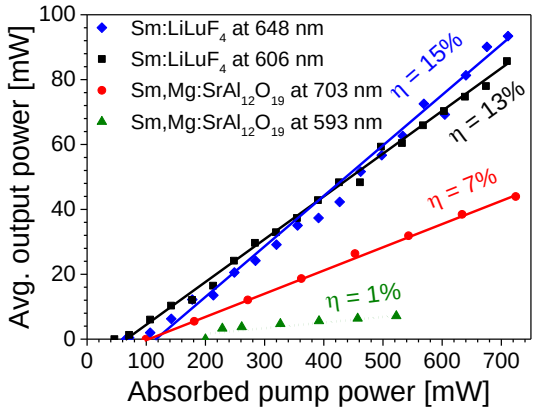

Figure 16: Laser characteristics of Sm^{3+}-doped $LiLuF_4$ and $SrAl_{12}O_{19}$ under pumping with a 2ω-OPSL emitting at 479.6 nm. It should be noted that the laser output was self-pulsed in all cases and the curve for Sm^{3+},Mg^{2+}:$SrAl_{12}O_{19}$ at 593 nm was obtained under chopped excitation in quasi-cw mode (dotted curve).

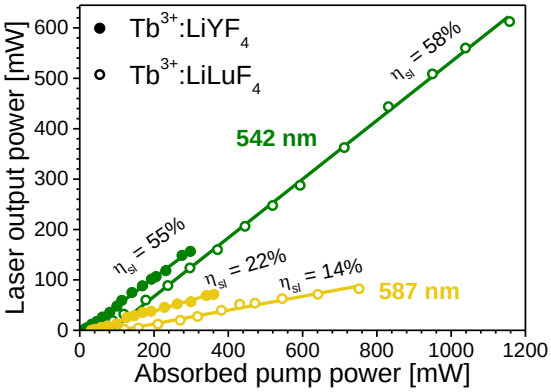

Figure 17. Laser characteristics of a 4.7 mm long Tb^{3+}(16%):$LiYF_4$ sample and a 11.4 mm long Tb^{3+}(14%):$LiLuF_4$ under pumping at 486 nm.[40] It should be noted, that the green Tb:$LiLuF_4$ laser was operated in a slightly different resonator configuration.

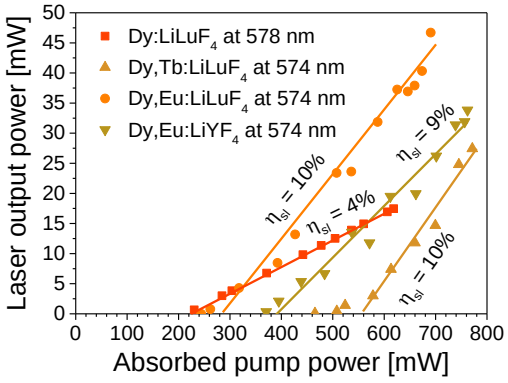

Figure 18: Laser characteristics of pure and co-doped Dy^{3+}:$LiLuF_4$ and Dy, Eu:$LiYF_4$ under pumping with an InGaN-laser diode at 450 nm. Without co-dopant, the laser operates in irregular self-pulsed operation (dashed line).[41, 61]

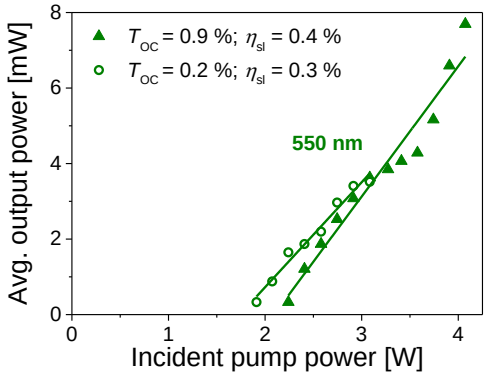

Figure 19: Laser characteristics of Ho^{3+}:LaF_3 under 2ω-OPSL-pumping at 479 nm.[46] It should be noted that the laser operated in a self-pulsed regime with a few µs pulse duration and several kHz repetition rate.

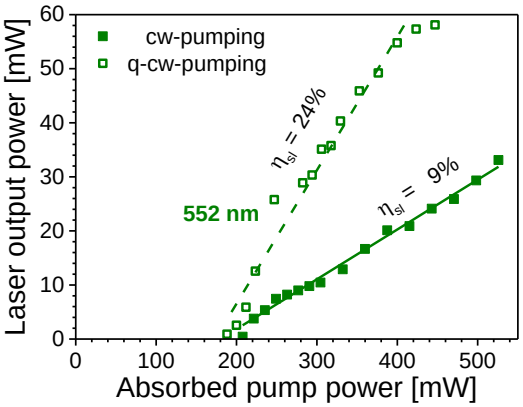

Figure 20: Laser characteristics of Er^{3+}:$LiLuF_4$ under cw and q-cw 2ω-OPSL-pumping at 486.15 nm.

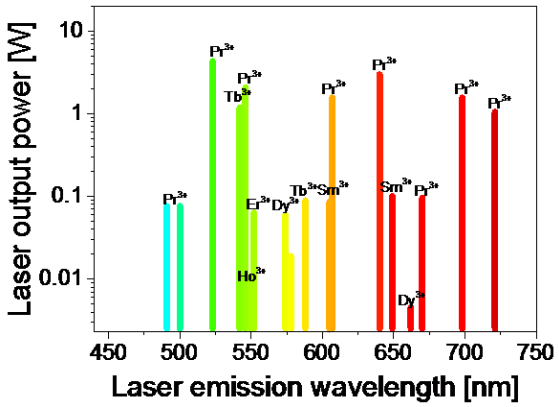

Figure 21: Laser output power vs. emission wavelength of Pr^{3+}-, Sm^{3+}-, Tb^{3+}-, Dy^{3+}-, Ho^{3+}- and Er^{3+}-doped materials (cf. Table 3). Many of the Pr^{3+}-lines depicted here allow for broad-band tuning (cf. Figure 11).

Tables

Ion	λ_{abs} [nm]	Transition	Pol.	σ_{abs} [10^{-21} cm²]
Pr^{3+}	441	$^3H_4 \rightarrow {}^3P_2$	σ	43
	444	$^3H_4 \rightarrow {}^3P_2$	π	102
	469	$^3H_4 \rightarrow {}^3P_1$	π	71
	479	$^3H_4 \rightarrow {}^3P_0$	π	234
Sm^{3+}	401	$^6H_{5/2} \rightarrow {}^6P_{3/2, 5/2}$	π	22
	463	Not assigned	π	3.4
	481	Not assigned	π	3.3
Tb^{3+}	488	$^7F_6 \rightarrow {}^5D_4$	σ	0.2
	489	$^7F_6 \rightarrow {}^5D_4$	π	0.3
Dy^{3+}	450	$^6H_{15/2} \rightarrow {}^4I_{15/2}$	π	1.4
	479	$^6H_{15/2} \rightarrow {}^4F_{9/2}$	σ	0.5
Ho^{3+}	450	$^5I_8 \rightarrow {}^5F_1 / {}^5G_6$	σ	36
	453	$^5I_8 \rightarrow {}^5F_1 / {}^5G_6$	π	38
	485	$^5I_8 \rightarrow {}^5F3$	σ	11
	486	$^5I_8 \rightarrow {}^5F3$	π	20
	535	$^5I_8 \rightarrow {}^5F_4 / {}^5S_2$	π	83
	537	$^5I_8 \rightarrow {}^5F_4 / {}^5S_2$	σ	16
Er^{3+}	405	$^4I_{15/2} \rightarrow {}^2H_{9/2}$	π	5.1
	440	$^4I_{15/2} \rightarrow {}^4F_{3/2}$	π	2.5
	450	$^4I_{15/2} \rightarrow {}^4F_{5/2}$	π	4.6
	486	$^4I_{15/2} \rightarrow {}^4F_{7/2}$	π	17

Table 1: Main absorption peaks of different rare-earth ions in $LiLuF_4$.[58-61]

Ion, τ(start level)	Final State	σ-polarization λ_{em} [nm]	σ-polarization σ_{em} [10^{-21} cm²]	π-polarization λ_{em} [nm]	π-polarization σ_{em} [10^{-21} cm²]
Pr^{3+} $\tau(^3P_J)$ = 0.05 ms	$^3H_4$	481	21	479	197
		491	7		
	$^3H_5$	538	7	523	24
		549	6	546	8
	$^3H_6$	607	118	605	93
		610	50	613	14
		618	13	618	7
		623	6		
		627	16		
	$^3F_2$	640	210	640	8
				645	12
	$^3F_3$	675	8	670	14
		680	12	691	6
		698	43		
	$^3F_4$			706	7
				710	7
		719	28	715	5
		730	11	721	72
Sm^{3+} $\tau(^4G_{5/2})$ = 4.6 ms	$^6H_{7/2}$			605	1.2
	$^6H_{9/2}$			649	0.7
	$^6H_{11/2}$	703	0.4		
Tb^{3+} $\tau(^5D_4)$ = 5.5 ms	$^7F_5$	542	1.3		
		544	1.6		
		548	0.5	548	0.5
	$^7F_4$			582	0.6
				588	1.1
	$^7F_3$			621	0.92
Dy^{3+} $\tau(^4F_{9/2})$ = 3.5 ms	$^6H_{13/2}$	574	1.7	568	0.9
		578	1.1	578	1.1
	$^6H_{11/2}$			662	0.6
Ho^{3+} $\tau(^5F_4, ^5S_2)$ = 0.1 ms	$^5I_8$			532	19.1
				550	5.4
				551	3.6
Er^{3+} $\tau(^4S_{3/2})$ = 0.37 ms	$^4I_{15/2}$			540	32
				552	27

Table 2: Radiative upper state lifetimes and main fluorescence peaks of different rare-earth ions in $LiLuF_4$.[30, 40, 42, 58-61]

	λ_{em} [nm]	Pol	Laser transition	η_{slope} [%]	P_{out} [mW]	P_{thr} [mW]	Operation mode	Pump source	Ref.
	491	σ	$^3P_J \rightarrow {}^3H_4$	6	70	285	cw	2ω-OPSL	[72]
	500	π	$^3P_J \rightarrow {}^3H_4$	7	70	200	cw	2ω-OPSL	[72]
	523	π	$^3P_J \rightarrow {}^3H_5$	72	2900	52	cw	2ω-OPSL	[73]
	523	π	$^3P_J \rightarrow {}^3H_5$	45	~4200	>500	cw	2×2ω-OPSL	[74]
	523	π	$^3P_J \rightarrow {}^3H_5$	62	773	148	cw	InGaN-LD	[75]
	546	π	$^3P_J \rightarrow {}^3H_5$	60	2000	120	cw	2ω-OPSL	[73]
	546	π	$^3P_J \rightarrow {}^3H_5$	52	384	728	cw	InGaN-LD	[75]
Pr^{3+}	605	π	$^3P_J \rightarrow {}^3H_6$	44	1500	114	cw	2ω-OPSL	[73]
	607	σ	$^3P_J \rightarrow {}^3H_6$	60	1400	185	cw	2ω-OPSL	[73]
	607	σ	$^3P_J \rightarrow {}^3H_6$	26	1500	1700	cw	4×InGaN-LD	[16]
	640	σ	$^3P_J \rightarrow {}^3F_2$	68	2800	17	cw	2ω-OPSL	[73]
	640	σ	$^3P_J \rightarrow {}^3F_2$	45	2900	~1000	cw	4×InGaN-LD	[16]
	670	π	$^3P_J \rightarrow {}^3F_3$	12	88	360	cw	InGaN-LD	[76]
	698	σ	$^3P_J \rightarrow {}^3F_{3,4}$	50	1500	65	cw	2ω-OPSL	[73]
	698	σ	$^3P_J \rightarrow {}^3F_{3,4}$	49	156	138	cw	InGaN-LD	[77]
	721	π	$^3P_J \rightarrow {}^3F_4$	53	1000	16	cw	2ω-OPSL	[73]
Sm^{3+}	605	π	$^4G_{5/2} \rightarrow {}^6H_{7/2}$	13	86	46	self-pulsed	2ω-OPSL	[32]
	649	π	$^4G_{5/2} \rightarrow {}^6H_{9/2}$	16	93	147	self-pulsed	2ω-OPSL	
Dy^{3+}	568	π	$^4F_{9/2} \rightarrow {}^6H_{13/2}$	-	-	-	self-pulsed	InGaN-LD	[61]
Dy^{3+},Tb^{3+}	574	σ	$^4F_{9/2} \rightarrow {}^6H_{13/2}$	13	55	320	cw	InGaN-LD	[41]
Dy^{3+},Eu^{3+}	574	σ	$^4F_{9/2} \rightarrow {}^6H_{13/2}$	10	47	244	cw	InGaN-LD	[61]
	578	σ	$^4F_{9/2} \rightarrow {}^6H_{13/2}$	4	17	188	self-pulsed	InGaN-LD	[61]
Dy^{3+}	580	σ	$^4F_{9/2} \rightarrow {}^6H_{13/2}$	-	-	-	self-pulsed	InGaN-LD	[61]
	661	π	$^4F_{9/2} \rightarrow {}^6H_{11/2}$	2	4	143	self-pulsed	InGaN-LD	[61]
Tb^{3+}	542	σ	$^5D_4 \rightarrow {}^7F_5$	52	1130	32	cw	2ω-OPSL	[40]
	544	σ	$^5D_4 \rightarrow {}^7F_5$	-	-	-	cw	2ω-OPSL	
	548	σ / π	$^5D_4 \rightarrow {}^7F_5$	-	-	-	cw	2ω-OPSL	
	582	π	$^5D_4 \rightarrow {}^7F_4$	-	-	-	cw	2ω-OPSL	
	587	π	$^5D_4 \rightarrow {}^7F_4$	22	71	32	cw	2ω-OPSL	
Ho^{3+}	550	π	$^5F_4$,$^5S_2 \rightarrow {}^5I_8$	0.4	8	2000	self-pulsed	2ω-OPSL	[46]
Er^{3+}	552	π	$^4S_{3/2} \rightarrow {}^4I_{15/2}$	9	33	207	cw	2ω-OPSL	[60]
	552	π	$^4S_{3/2} \rightarrow {}^4I_{15/2}$	24	58	188	q-cw	2ω-OPSL	

Table 3: Selected laser results obtained with $LiLuF_4$ or $LiYF_4$ doped with different rare-earth ions under pumping with blue-emitting semiconductor-based pump sources.

Author biographies

Christian Kränkel received his PhD degree in 2008 at the Universität Hamburg, Germany. After a postdoctoral position at the ETH Zürich, Switzerland, he became a junior group leader at the Universität Hamburg in 2010, where he joined the Institut für Laser-Physik. His current fields of research include the growth and characterization of crystalline laser materials for lasers with emission wavelengths from the UV to the mid-IR spectral range in cw and pulsed operation mode.

Daniel-Timo Marzahl studied physics at the Universität Hamburg in Hamburg, Germany and received his diploma degree 2012 in the solid-state laser group of Prof. Dr. Günter Huber. Since then he pursues his studies towards his PhD in the same group. His current research topics are growth, spectroscopy and laser characterization of rare earth-doped laser materials for laser operation in the visible spectral range.

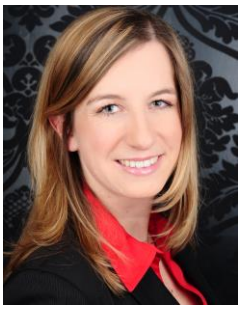

Francesca Moglia received her Master degree in Physics in 2008 at the University of Pisa in Italy. In 2013 at the Universität Hamburg in Germany she completed her PhD studies concerning the investigation of new upconversion materials and the development of upconversion lasers. Currently, she is a postdoctoral researcher at DESY (Hamburg, Germany) dedicated to the development of a laser amplifier and the stable operation of the injector laser for the new European XFEL.

Guenter Huber received his Ph.D. degree in physics from Stuttgart University/Germany in 1975. He was staff member of the Max-Planck-Institute/Stuttgart and the Universität Hamburg. In 1982 he became Professor of Physics at Universität Hamburg, where he served as Director of the Institut für Laser-Physik, as Dean of the Physics Faculty, and member of the University Council. His research is focused on solid-state lasers, the growth and fundamental characterization of new laser crystals. He is Fellow of OSA, EPS and received the Quantum Electronics-Optics Prize of EPS and the Charles Hard Townes Award of OSA.

Philip Metz received his diploma in physics in 2011 at the Universität Hamburg in Germany, where he also performed his PhD thesis on visibly emitting solid state lasers until 2014. Afterwards, he continued with this topic at the Universität Hamburg as a postdoctoral researcher. In 2016 he went to Coherent LaserSystems GmbH & Co. KG where he develops solid state lasers.

Graphical Abstract

The current state of visible rare-earth doped crystalline lasers under pumping with novel blue semiconductor-based pump sources is reviewed. Spectroscopy and laser results of Pr^{3+}-, Sm^{3+}-, Tb^{3+}-, Dy^{3+}-, Ho^{3+}-, and Er^{3+}-doped laser materials are presented.

ToC figure